UNIVERSITY OF NOVA GORICA
SCHOOL OF APPLIED SCIENCES

IMPACT OF LONGITUDINAL ELECTRON BEAM PROPERTIES ON FREE ELECTRON LASER EMISSION: THE CASE STUDY OF FERMI@Elettra

DIPLOMA THESIS

Matija Stupar

Mentors: prof. Dr. Giovanni De Ninno
Dr. Giuseppe Penco

Nova Gorica, 2013

UNIVERZA V NOVI GORICI
FAKULTETA ZA APLIKATIVNO NARAVOSLOVJE

VPLIV LONGITUDINALNIH LASTNOSTI ELEKTRONSKEGA SNOPA NA EMISIJO LASERJA NA PROSTE ELEKTRONE: **PRIMER ŠTUDIJE NA FERMI@Elettri**

DIPLOMSKO DELO

Matija Stupar

Mentorja: prof. Dr. Giovanni De Ninno
Dr. Giuseppe Penco

Nova Gorica, 2013

Acknowledgement

Credits for guidance, help and an opportunity to enter a challenging world of science at FERMI@Elettra goes to my mentors, prof. Dr. Giovanni De Ninno and Dr. Giuseppe Penco. I am also grateful for the help provided by David Gauthier for discussions of the results and calculations, Eugenio Ferrari for providing software and modifications that helped me to carry out the analysis of the data. Final thanks go to my family for a generous amount of patience.

Abstract

Free-electron lasers (FEL's) are coherent and tunable light sources, whose spectral range varies from far infrared to the X-rays. They offer unique opportunities for scientific applications in various scientific domains, from fundamental physics to biology, medicine, chemistry and material science. In a FEL, a relativistic electron beam interacts with the magnetic field provided by an undulator. This forces particles to move along periodic trajectories and, consequently, to emit radiation. When a proper resonant condition is met, the radiation is then amplified, until the laser effect is reached. Sincrotrone Trieste is presently engaged in the commissioning of a new FEL, named FERMI@Elettra, covering the spectral range between 85 and 10 nm. FERMI@Elettra is the first user facility based on the principle of seeded harmonic generation (HG). In a seeded FEL, the electron beam primarily interacts with an external coherent light signal (the seed). As a result, electrons get spatially modulated and become able to emit coherent radiation at the harmonics of the seed. Longitudinal coherence is instead not achieved in unseeded FEL's. The process of HG is very sensitive to the electron-beam characteristics and, in particular, to the current and energy distributions along the beam. Studying experimentally the impact of the local properties of the beam current and energy profiles (e.g., current uniformity and energy chirp) on the features of the FEL light (e.g., intensity, wavelength and bandwidth) is essential for understanding the fundamental principles of the FEL process and, therefore, for controlling the latter in view of user experiments.

Povzetek

Laserji na proste elektrone (eng. FEL) so koherenten in nastavljiv svetlobni vir, s spektralnim razponom od infrardečih do rentgenskih žarkov. Ti svetlobni viri ponujajo edinstvene priložnosti za uporabo v različnih vejah znanosti, od fizike osnovnih delcev do biologije, medicine, kemije in raziskavah materialov. V laserju na proste elektrone snopi elektronov, ki tvorijo elektronski žarek interagirajo z magnetnim poljem undulatorja. Sile pri tej interakciji prisilijo elektrone v gibanje po periodičnih trajektorijah zaradi česar slednji izsevajo svetlobo. Ko so izpolnjeni določeni pogoji resonance se izsevana svetloba ojača dokler ni dosežen laserski efekt. Sincrotrone Trieste trenutno izvaja diagnostiko in optimizacijo novega laserja na proste elektrone imenovanega FERMI@Elettra, namenjenega proizvajanju svetlobe z valovnimi dolžinami med 10 in 85nm. FERMI@Elettra je prvi obrat ki temelji na principu generiranja harmonikov namenjen uporabnikom. V laserju na proste elektrone ki temelji na principu sejanja, elektroni primarno interagirajo z zunanjo koherentno svetlobo (semenom). Pod vplivom zunanjih električnih polj se elektroni periodično prostorsko porazdelijo. Posledično so zmožni oddajati koherentno svetlobo v harmoničnih frekvencah sejalnega laserja, medtem ko pri laserjih na proste elektrone brez principa sejanja ne dobimo koherentne svetlobe. Princip generiranja harmonikov je zelo občutljiv na lastnosti elektronskih snopov, še posebej na tokovno in energijsko distribucijo znotraj gruče elektronov. Eksperimentalne študije vpliva lokalnih lastnosti gruče elektronov (npr. tokovne in energijske neenotnosti) na lastnosti emisije laserja na proste elektrone (npr. intenziteta, valovna dolžina in pasovna širina) so zato ključne za razumevanje osnovnih principov le tega. Pomembne so tudi za bodoče eksperimente.

INTRODUCTION

In modern science that focuses on the study of nanoscale structures and fast phenomena, there is a rising need of light sources generating intense ultra-short pulses (less than one picosecond), in the XUV spectral range. Free electron lasers (FELs) are currently the only light sources fulfilling all these requirements.

According to Maxwell's equations, accelerated electrons emit radiation. If the electron energy is relativistic, this radiation becomes directional and thus the radiated flux through a given (small) area is enhanced. Synchrotrons and storage rings take advantage of this phenomenon by bending the trajectory of electrons in the magnetic field of a dipole magnet. However, this has proved not to be optimal since dipole radiation is emitted in a broad angle such that only a small portion of light could be used for experiments. Nowadays synchrotron storage rings use undulators: an array of periodic permanent magnets that force the electrons to oscillate. Thus, radiation is emitted in a much smaller angle, and this further enhances the photon flux.

Linac-based FEL light sources aim at providing radiation with pulse lengths of near hundreds of femtoseconds in the soft and hard X-ray range. The advantage of FELs compared to storage rings is that their linear design allows the emitted light to travel together with the relativistic electron bunch, over long distances. The light-electron coupling is responsible for light amplification and, eventually, for FEL emission. If the amplification of the propagating wave is achieved in a single passage of electron beam, the configuration is called single pass configuration.

There are two different schemes that can be distinguished in single pass FEL's, based on the origin of radiation used to initiate the FEL process. The first one is called Self-Amplified Spontaneous Emission (SASE) where the FEL process is generated by the shot noise in the electron bunch density distribution and then amplified all along the undulator. The second configuration is called Coherent Harmonic Generation (CHG), (see section 2.3.1) [7]. In a CHG process an initial seed signal is provided by a conventional high-peak power pulsed laser operating at wavelengths in the region of 240-300nm at the electron bunches repetition frequency. The seed laser is temporally synchronized to overlap the electron beam, produced by the linac accelerator, in a

first undulator section called the modulator. The laser field modulates the transversely wiggling electron bunch energy at its own frequency. This energy modulation is then converted to bunch charge spatial density modulation by passing the electrons through a chromatic dispersive section. The resultant density modulation contains higher harmonics of the seed laser wavelength. A subsequent set of undulator sections, known as radiators, is tuned in magnetic strength so that intense, coherent FEL radiation at a wavelength corresponding to one of these harmonics is emitted and then amplified to a high peak power level. The FEL radiation will have approximately the temporal duration of the seed laser and the polarization properties of the radiator undulators.

However, in order for an FEL source to reach the best performance, one must overcome many physical and technical challenges. As an example, it is very difficult to create an electron bunch with a constant energy profile perfectly matching the resonant condition and a seed laser with a very short pulse length and fully monochromatic (see section 2.2.1). More often the electron beam has a peculiar energy distribution along the bunch and the seed laser has a frequency time dependence, named frequency chirp, that affect the FEL output properties, as inducing a broadening of the FEL spectrum. The goal of this thesis is to experimentally explore the interplay between the electron energy temporal profile and the seed laser frequency chirp, searching for a possible compensation of these two contributions for producing a narrow bandwidth FEL pulse.

The study was carried out at the FERMI@Elettra machine, that is a single-pass FEL based on the seeded high-gain harmonic generation (HGHG) scheme which will be described in details in the chapter 3.

1.1 Outline of the thesis

The thesis is organized as follows: the second chapter provides an overview on the acceleration of electron bunches, of light generation using an undulator and on the principles on which seeded FELs rely. Chapter three includes a description of the FERMI facility, with a particular focus on the diagnostics and experimental methods

used in our experiments; the concepts of laser and electron chirp are introduced in chapter four, together with the theoretical description of the compensation of electron energy profile using a certain frequency variation along the laser pulse. The fifth chapter includes the measurement methods and analysis of results, obtained for different laser chirp values and is also devoted to the discussion of the obtained results and to eventual experiments that will be carried out in the near future.

1.2 FELs: State of the art

Between 1957 and 1964, early SASE FELs started to be developed at microwave and infrared wavelengths, and were using relatively small electron energies and high currents [1].These experiments demonstrated much of the essential physics for further development of FELs. Later from 1997 to 2002, the experiments at Low Energy Undulator Test Line (LEUTL) at Argonne National Laboratory were the first, to demonstrate SASE in the visible and UV range. SASE proved to be a great and simple way to obtain short wavelengths (x-ray) and peak powers in orders of GW. However shot to shot noise in the longitudinal electron density distribution responsible for initial spontaneous undulator emissions in SASE, result in fluctuations in the output spectrum and intensity. An alternative to SASE has been introduced using a seed laser in order to create a desired frequency to start a chain of harmonic amplifications (CHG section 2.2.1), also capable of creating temporally coherent pulses.

Below the current status of FEL light sources will be described, focusing particularly on single-pass FELs, since this is the configuration used at FERMI@Elettra. Some prototypes have been realized in the recent past in order to test both the SASE and harmonic generation principles. Among experiments the in SASE regime, LEUTL (Advanced Photon source ,Argonne, USA) has reached the 530nm (2000)[2]; VISA (Visible to Infrared SASE Amplifier) at Accelerator Test Facility of Brookhaven National Laboratory (USA) produced FEL radiation at 840nm (2001) [3]; TTF(Tesla Test Facility)[or FLASH (Free-electron LASer in Hamburg)] at DESY (Germany), reached 4.12nm (2010)[4]; SCSS (Spring-8 Compact SASE Source) at Stanford (USA)reached 0.15 nm (2009) [5]. The High Gain Harmonic Generation (HGHG), scheme has been tested at Deep Ultra Violet – FEL (National Synchrotron Light

Source, BNL, USA) and reached harmonic radiation at 193nm in (2006)[6]. Seeding was achieved at SPARC FEL and they reached 197nm in 2010[6]. Another facility based on the seeded configuration is FERMI@Elettra which reached 4nm using FEL-2 in 2013 [7].

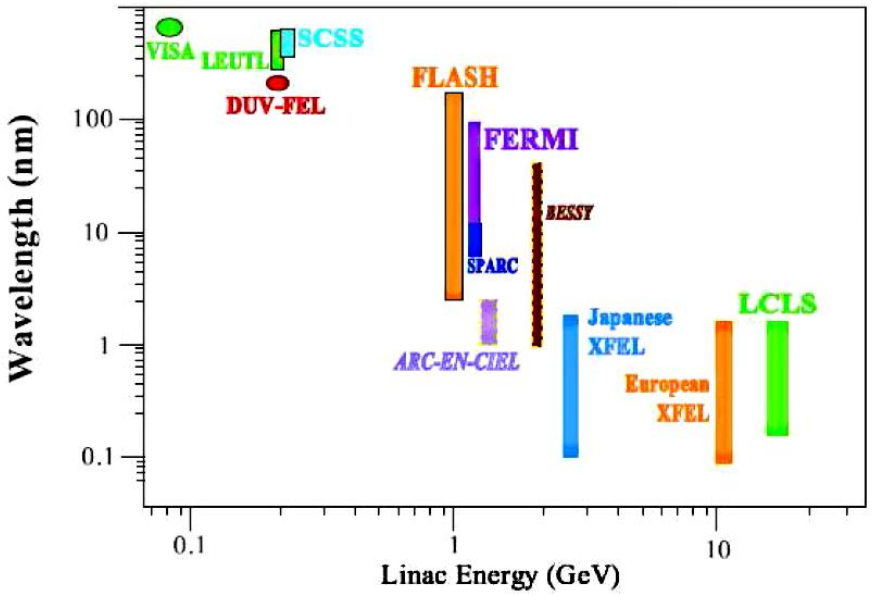

Figure 1.1 Target wavelength and linac energy of present and future FELs in single pass configuration

In fig.1.1 [8] there is a comparison of wavelength ranges and linac energies of present and future FEL projects. These are now the next step light sources compared to 3rd generation synchrotron storage rings. The peak brightness (defined as the number of photons per pulse per unit solid angle, emitted from the unit surface of the source in a given frequency band) of FELs is orders of magnitude higher than that of storage rings, as shown in Fig. 1.2 [8].

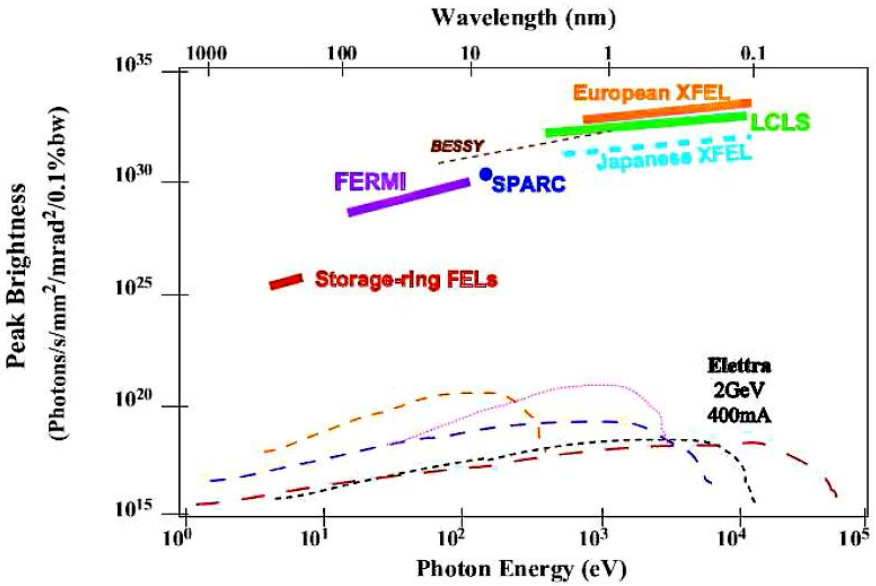

Figure 1.2 Comparison of X-FEL projects, 3rd generation synchrotron light sources and storage-ring FELs

Storage ring FELs based on seeded single pass configuration has been implemented only a few times, at UVSOR (Okazaki, Japan) [9] and Elettra SRFEL [10]

2. FEL PHYSICS

2.1 Electron beam acceleration

In order to obtain relativistic electrons ready to emit light we need to accelerate and guide them through a predefined path of magnetic and electric fields. Particle beams have properties similar to light and tend to spread, thus focusing devices such as quadrupoles must be placed along the entire beam transport line to match the transverse beam properties (i.e. the optics parameters), to the design pattern. Although the transverse phase space is very important in electron beam dynamics, this thesis is focused on the longitudinal phase space implication on the FEL performance.

In general [11] a charged particle with charge q and velocity $\vec{v}$ in the electromagnetic fields $(\vec{E}, \vec{B})$, is exerted by the Lorentz's force $\vec{F}$:

$$\vec{F} = q(\vec{E} + \vec{v} \times \vec{B}). \tag{2.1}$$

The charged particle can only gain or lose its energy by its interaction with the electric field $\vec{E}$.

Accelerators are composed of ion sources, cavity and magnet components that can generate and maintain electromagnetic fields for beam acceleration and manipulation, devices to detect beam motion, high vacuum components for attaining excellent beam lifetime, undulators and wigglers to produce high brilliance photon beam, targets for producing secondary beams, etc. [11] Accelerators can be classified as linear or circular, electrostatic of radio frequency, continuous or bunched and pulsed. In particular FERMI is a RF linac operating with a repetition rate of 10 Hz, devoted to accelerating electron bunches of 500-800 pC. The linac is composed by a series of travelling wave sections, such as the one presented in fig.2.1 resonating at 3 GHz. A complete description will be provided in the chapter 3. Traveling wave accelerators [12] are basically RF waveguides where the electromagnetic field travels with a phase velocity equal to that of the injected beam. Therefore, the beam is locked to the

traveling wave with a consequently linear energy gain along the structure. In order to match the phase velocity of the RF wave with the travelling electron beam, it is necessary to load the traveling wave structure with metallic discs along its axis.

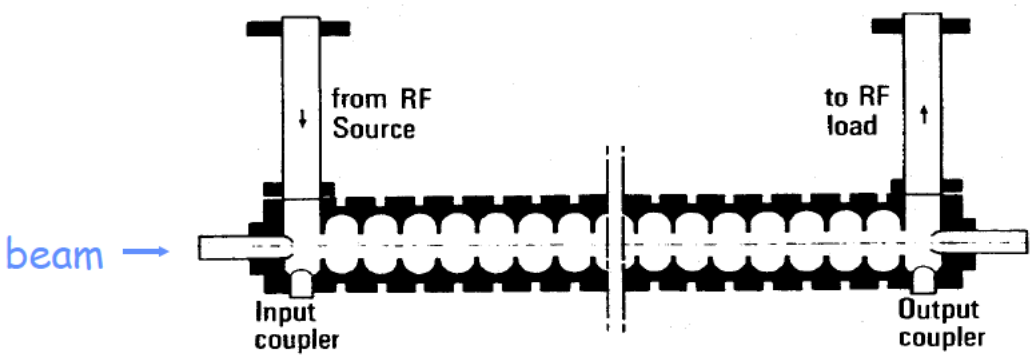

Figure 2.1 Scheme of a traveling wave linac [13]

2.2 Undulator

An undulator is a periodic permanent magnet structure with period λ_u [14] and it is designed to induce transverse oscillation of electrons, which thus lose kinetic energy by emitting photons. A schematic view of an undulator is shown in fig. 2.2.

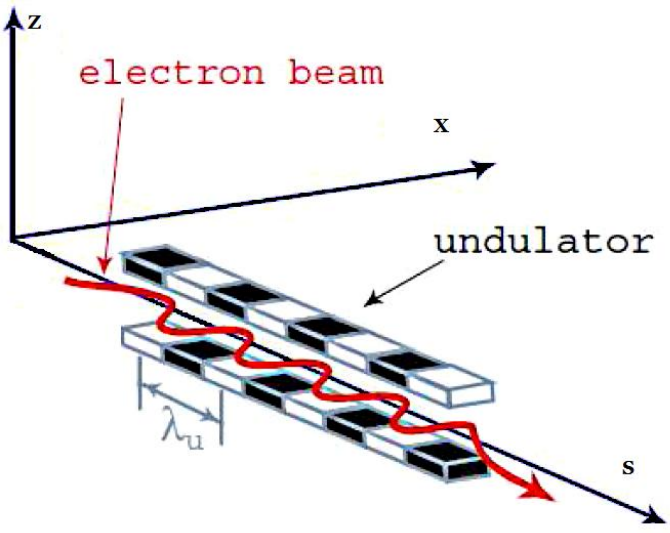

Figure 2.2 Schematic view of an undulator

The emitted radiation from an undulator has a frequency well defined by its period λ_u, the energy of electrons and the strength of the magnetic field generated by undulator poles. Since the electrons oscillation period is the same as the undulator

magnet structure, they emit radiation fields that are coherently superimposed, generating an high intensity radiation that is almost monochromatic. The central wavelength of an undulator is given by [15]

$$\lambda_k = \frac{\lambda_u}{2\,n\,\gamma^2}\left(1 + \frac{1}{2}K^2 + \gamma^2\vartheta^2\right), \tag{2.2}$$

where n is the order of harmonic, K is the magnetic deflection parameter, modulated by the undulator gap, γ is the electrons Lorentz factor, and ϑ is the angle of emission with respect to the electron propagation axis. Since, in general only forward direction is considered this last term can be neglected. We can also note that the shortest wavelength is emitted in the forward direction. For an undulator with finite number of periods N_p these spectral lines have a width proportional to $1/N_p$.

2.3 Free electron laser

A common principle for all FELs is the Lorentz force interaction between relativistic electrons and the co-propagating electric field. Energy transfer is possible if the electron performs oscillations that induce a transverse velocity component. This transverse velocity component then interacts with the transverse component of the electric field resulting in energy transfer between the electrons and the wave. Energy can be transferred both ways, from the wave to the electrons, when the electron energy is modulated by the wave, or from the electrons to the wave, when we want electrons to contribute energy to the wave, resulting in an overall radiation gain. Energy exchange reaches its peak when the maximum of the electric field is in phase with the maximum transverse velocity of the electron. In linear accelerators such as FERMI, the energy of the electrons is not restored once they leave the linac. Since the electrons transfer energy to the electric field of the laser, the system reaches saturation when electrons lose enough energy to fall out of the resonance condition.

Two main FEL configurations can be distinguished: the single pass configuration, where the amplification of the electromagnetic wave occurs in one passage through the undulator, and the oscillator configuration, in which the electromagnetic wave is stored in an optical cavity and lasing is achieved as the result of a large number of light-electron interactions inside the undulator.

In a high-gain single-pass FEL [16], light amplification results from this resonant coupling between an ultra-relativistic electron beam guided by the static and periodic magnetic field generated by a long undulator and a co-propagating electromagnetic wave. As a result of the interaction between the electrons and the electromagnetic field, the beam is modulated in energy, with the period of the modulation being equal to the wavelength of the electromagnetic field. As the beam propagates further inside the undulator, the energy modulation naturally transforms into a spatial modulation of the electron density at the fundamental wavelength. As a result, the electron beam is subdivided into microbunches that emit in phase, [8] producing FEL radiation which is almost Fourier transform limited, has a high flux and can be tuned over a wide range of wavelengths (from angstroms to hundreds of nanometers). In some configurations this radiation also has a variable polarization.

2.3.1 Harmonic generation

Single pass FEL light sources such as FERMI@Elettra are based on seeding technique. [14] Seeding relies on the use of an external laser source.

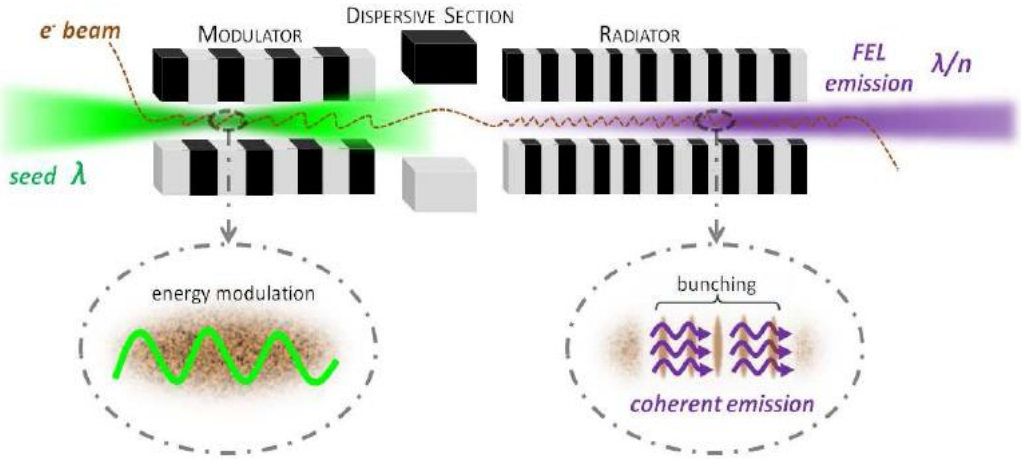

Figure 2.3 Scheme of seeded harmonic generation [14]

The layout of a seeded FEL presented in fig.2.3 is made out of two undulators (modulator and radiator) separated by a dispersive section. In the first undulator (modulator) the interaction between the laser electric field and the electrons occurs in

the conditions [8] that maximize the exchange of energy between the particles and the external fields. The electrons are randomly distributed before they enter the modulator, while at the end of the modulator there is a periodic energy modulation in the bunch caused by the external field. In order to obtain such modulation the seed laser pulse must be significantly stronger than the spontaneous emission of electrons as they enter the modulator. Energy modulation is converted to spatial modulation in the dispersive section (see section 2.3.2). This process of periodic spatial distribution is also called microbunching [14]. The bunched pulse then enters the second undulator known as the radiator which must be tuned to one of the harmonics of the seed wavelength in order to fulfill the resonance condition. The resonance condition is met when the electrons and the wave remain in phase all along the undulator [15]. Since the electrons always move slightly slower than the wave and also follow a curved path inside an undulator the difference in path must be set to the wavelength of the emission. When the microbunched electron beam enters the second undulator the microbunches behave and emit radiation as macro-particles resulting in a powerful coherent emission.

2.3.2 Dispersive section

The dispersive section is a chicane that drives electrons with different energies along different paths. As mentioned in section 2.3.1, energy modulation achieved by seeding process is turned into spatial modulation in this dispersive section.

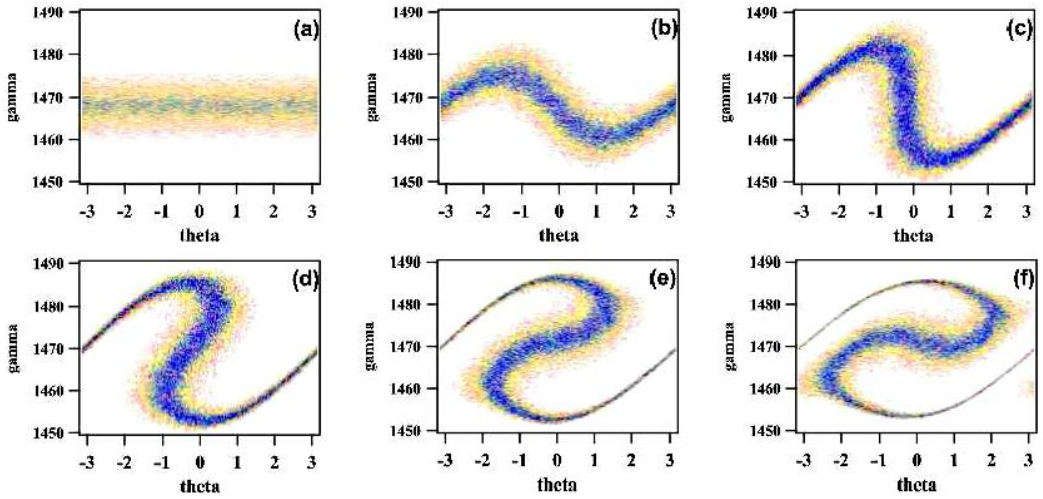

Figure 2.4 Evolution of the electron-beam phase space in the process of beam bunching. a) initial distribution b) energy modulation c) spatial modulation d,e,f) overbunching [14]

The process of creating this spatial modulation can be better explained using figure 2.4. At the beginning of the modulator (a) the electrons in the beam have a random phase with respect to the seed laser field. Then the exchange of energy between the seed laser field and the electrons inside the undulator, induces energy modulation, this energy modulated bunch (b) is now guided through a dispersive section. As previously mentioned the dispersive section is a magnetic chicane that causes electrons with different energies to follow different paths. In the ideal case the more energetic electrons from the top position in fig.2.4 (b) end up at the same position as the less energetic ones, causing a spatial distribution (c), the process of creating such spatial distribution is called bunching. The distance between successive bunches (fig.2.4 shows slices of only one length λ) is around the wavelength of the seed. Such an increase in electron content around a certain position causes the beam to emit as a group of macro-particles, resulting (under proper undulator settings) in the coherent emission. If the process of spatial modulation inside the dispersive section is too strong overbunching occurs as shown in (d), (e) and (f). Over bunching is present if the power of the seed is too strong for a particular strength of dispersive section, in this case we obtain energy profiles as shown in (d), (e) and (f). Over bunching reduces the effect of electrons emitting as macro-particles and thus depresses the coherent emission in the radiator and can also lead to spectral broadening Without coherence the intensity of FEL emission is greatly reduced.

The next chapter is an overview of the FERMI FEL, the machine where our experiments were carried out.

3. THE FERMI LIGHT SOURCE

The FERMI@Elettra [17] single-pass linac-based FEL is one of the FEL based European projects, designed to become the international user facility in Italy for scientific investigations of ultra-fast and ultra-high resolution processes in material science and physical biosciences with ultra high brilliance X-ray pulses. With a peak brightness of about ten orders of magnitude higher than third generation sources (see fig.1.2), full transverse coherence, close to transform limited bandwidth, pulse lengths of the order of a picosecond or less, variable polarization and energy tunability, the FERMI source is a powerful tool for scientific exploration in a wide spectrum of disciplines. The FERMI facility comprises two separate coherent radiation sources, FEL-1 and FEL-2. FEL-1 which was commissioned from 2009 to 2012, is based on a single cascade harmonic generation, [16] and has now been running for the users beamlines experiments successfully in the wavelength range between 100 and 20nm. FEL-2 is designed to operate at shorter wavelengths (20-4nm) via a double cascade mechanism. [14]

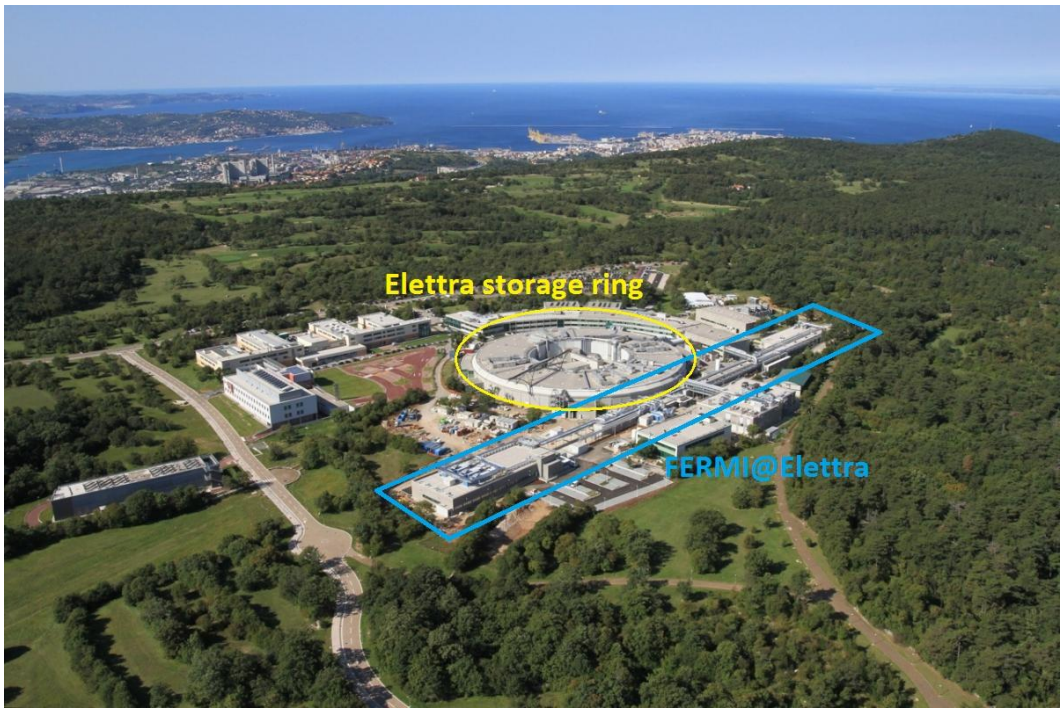

Figure 3.1 Aerial view of FERMI@Elettra facility (blue) and Elettra storage ring

As previously mentioned FERMI light source consists of a linear accelerator an undulator hall with two principal FEL lines: FEL-1 and FEL-2. The linear accelerator

accelerates particles up to energies of 1.2 GeV and 1.5 GeV. For that, use is made of a photoinjector laser with a wavelength of 261 nm. The photoinjector laser pulse has a Gaussian temporal profile and spectrum. A more detailed description of the photoinjector laser and the linear accelerator will be done in the following sections.

3.1 General layout

A general layout [17] of the facility is shown in Fig.3.2. The accelerator (Fig3.2 brown part) and FEL complex comprises the following parts: a photoinjector and two short linac sections (LINAC 0) generating a high brightness ~100 MeV electron beam [18] (first 10 meters), the main linear accelerator (LINAC 1-4) in which the beam is time-compressed and accelerated up to ~ 1.5 GeV (170 meters), [19] the system to transport the beam to the undulators, the undulator complex (Fig.3.2 green part) generating the FEL radiation (270 meters long), the photon beamlines taking the radiation from the undulator to the experimental area and the experimental area itself [17].

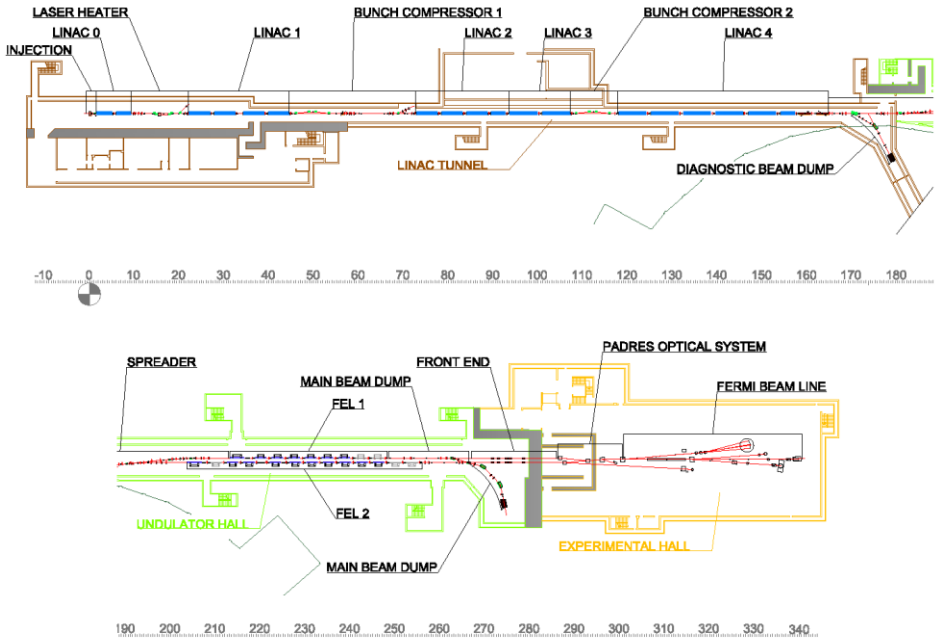

Figure 3.2 FERMI layout, Linear accelerator (brown), undulator hall (green) and experimental hall (yellow)

After leaving the undulators, while the FEL radiation is transported to the experimental areas (Fig3.2 yellow part), the electron beam is brought to a beam dump by a sequence of bending magnets. The FEL radiation transport system also described in section 3.4, is designed to handle the high peak power of up to 10 GW in the sub-picosecond pulse durations, includes a differentially pumped windowless vacuum system and low-Z material beam-line components operating at grazing incidence angles. The photon beam transport and diagnostics is carried out by the optical station (named PADRES) for light beam diagnostics and distribution to the user beamlines [20].

Parameters	*Value at 40 nm*	*Value at 10 nm*	*Units*
Electron beam energy	1.2	1.2	GeV
Peak current	800	500	A
Emittance (slice)	1.5	1.5	μm, rms
Energy spread (slice)	150	150	keV
Bunch duration	700	1400	fs, FWHM
Repetition rate	10	10	Hz
FEL peak power	2.5	0.6	GW
FEL pulse duration	200	400	fs, FWHM
# of photons/pulse	10^{14}	10^{12}	
Bandwidth	17	4	meV
Brilliance	~10^{31}	~10^{31}	ph/s/mm²/mrad²/0.1%BW

Figure 3.3 Main beam and pulse parameters FEL-1

As mentioned above, the FERMI@Elettra facility comprises of two separate coherent radiation sources, FEL-1 and FEL-2. In Fig.3.3 one can see the nominal machine parameters for FEL-1. Concerning the electron beam, fig. 3.3 reports the energy at the end of the linear accelerator, the peak current that is the maximum current of the beam, the slice energy spread that is the local energy spread of the beam (see section 4.2),the bunch duration that is the full-width half maximum temporal electron bunch length. Concerning the FEL radiation it is reported the repetition rate that is the number of pulses that the FEL produces per second, the FEL peak power that is the maximum power of the emitted beam, the "# of photons" that is the total pulse photon content, the bandwidth that is the spectral width of the emitted pulse, and the brilliance that is the brightness parameter also used in section 1.2.

3.2 Linear accelerator

The first part of the FERMI facility is the linear accelerator. The first element is the photoinjector [18] (purple structure in Fig 2.4). One of the requirements for a photoinjector dedicated to a scientific user facility such as FERMI is reliability and constant quality of the generated electron beam. Gun cavity dimensions were carefully designed in order to control the resonant frequency of the accelerating field. It is based on the proven electron gun [17], developed at BNL/SLAC/UCLA and delivered by UCLA in 2008. The nominal bunch is ~8ps (FWHM) long with a total charge of 500 pC. By optimizing the RF gun parameters, the solenoid strength and the laser driven parameters (transverse and longitudinal profile), a very high brightness beam has been routinely produced, with a normalized transverse emittance of about 0.65mm mrad and a peak current of ~60 A. This electron beam is accelerated to about 100MeV by the accelerating booster sections (fig. 3.4 (L0)). Several bunch compression configuration have been tested for the FERMI FEL operations in order to alternatively accomplish the requirement of a high peak current (500-600 A) needed to have sufficient emission or of a long electron bunch (~1ps), as requested in for double pulse seeding in FEL-2: (i.e. the electron bunch in this configuration has to be long enough to accommodate the two seed laser pulses having a temporal separation of several hundreds of fs). Moreover in a general mode of operation the current and energy profile along the bunch must have a flat-top profile in order to meet the proper matching condition for sustaining and enhancing both FEL pulses processes. In order to linearize the longitudinal compression and obtain a flat current profile, use has been made of fourth-harmonic RF cavity (X-band cavity [21]) installed before a magnetic chicane. It has been operated at a gradient of about 17MV/m and close to the maximum decelerating phase to compensate for the non linear term due to the RF curvature of the linac upstream of the chicane and to the second order momentum of the chicane itself. After the compression of the electron bunch, the longitudinal wakefields generated in the downstream linac sections modify the beam energy distribution, inducing a positive quadratic chirp in the longitudinal phase space. Using a high energy RF deflecting cavity (HERFD) installed at the linac end combined with an energy spectrometer allows measuring the longitudinal phase space (see section 4.2), making it possible to tune the X-band

phase and amplitude to flatten the current profile and to set the accelerating cavity phases to manipulate the beam energy distribution.

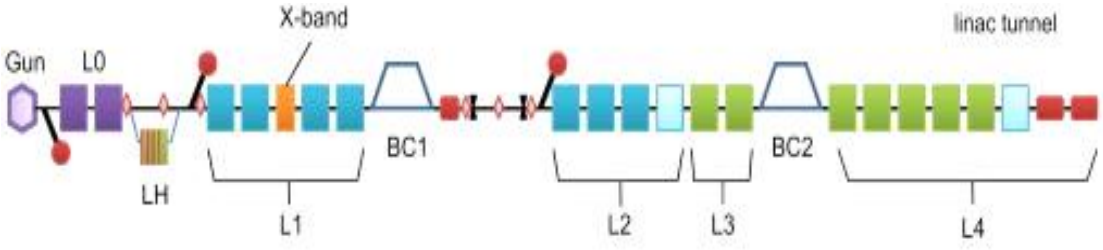

Figure 3.4 The FERMI@elettra FEL linear accelerator schematic view L(0,1,2,3,4) are linac cavities, BC(1,2) are the two bunch compressors.

Figure 3.5 Part of FERMI@elettra FEL linear accelerator

Figure 3.5 shows the beginning of the linear accelerator with two booster linacs (blue), and laser heater setup.

3.3 Undulators

FEL-1 and FEL-2 [17] are required to provide, at all wavelengths, continuously tunable beam polarization ranging from linear-horizontal to circular and linear-vertical. The FEL-1 radiator and the final radiator in FEL-2 have therefore been chosen to be of APPLE-II type [17]. This type of undulators can change the polarization by changing the longitudinal position of the magnetic array. For the modulator a simple, linearly-polarized configuration is best, due to both its simplicity

and the fact that the input seed radiation can be linearly polarized. The wavelength is tuned by changing the undulator gap at constant electron beam energy (see eq.2.2). The FEL-1 and FEL-2 radiators consist of 6 and 8 undulator magnets, respectively. Electromagnetic quadrupoles, beam position monitors, and quadrupole movers are installed in between undulators to correct the electron trajectory.

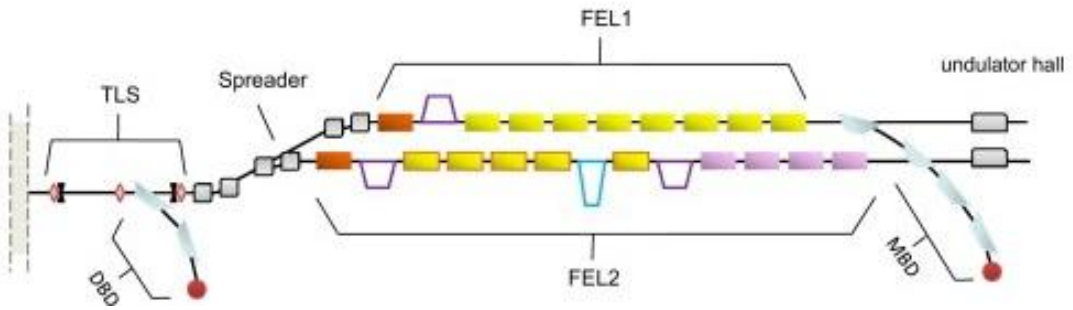

Figure 3.6 The FERMI@elettra FEL undulator hall, schematic view

Fig.3.6 shows the schematic view of both undulator lines FEL1 and FEL2. Measurements of longitudinal phase space properties explained in section 4.2, were performed in the DBD (diagnostic beam dump) as shown in the upper figure, while FEL spectra were acquired in the undulator hall. The orange block of fig 3.6 is the modulator, the purple chicane afterwards is the dispersive section and the yellow blocks are the undulators (radiators). Wavelength tuning using an undulator at fixed electron energy is limited by the minimum undulator gap, the strength of the magnetic field at the tip of the undulator poles and the undulator wavelength. The modulator for FEL-1 must satisfy FEL resonance for a nominal seed wavelength of 240 to 360 nm, the selected undulator wavelength is 26 cm. When choosing the radiator wavelength, there are two main requirements. First the FEL resonance must be possible for the longest desired output wavelength, which requires small gaps and long radiator periods. The second requirement is to have a reasonable gain at the shortest desired output wavelength, requiring a shorter radiator period. As can be seen from eq. 2.2, if one tries to change the undulator wavelength towards shorter wavelengths, strength of the magnetic field K must be decreased, by decreasing K we effect the gain, and reduce the final output power of radiation. Considering both requirements the chosen wavelength for the FEL-1 radiators was 55mm.

3.4 Experimental hall

The radiation [17] coming from both FEL lines is analyzed in terms of intensity, position and spectral content, giving online and shot to shot information to the users. A gas-based cell also referred to as an IO monitor gives the possibility to control the flux delivered to the beamlines. The transport system carries the beam to the end stations; it includes a beam splitting and delay section and the different refocusing mirror chambers. The System responsible for all of these operations is called PADReS, which stands for Photon Analysis Delivery and Reduction System [20].

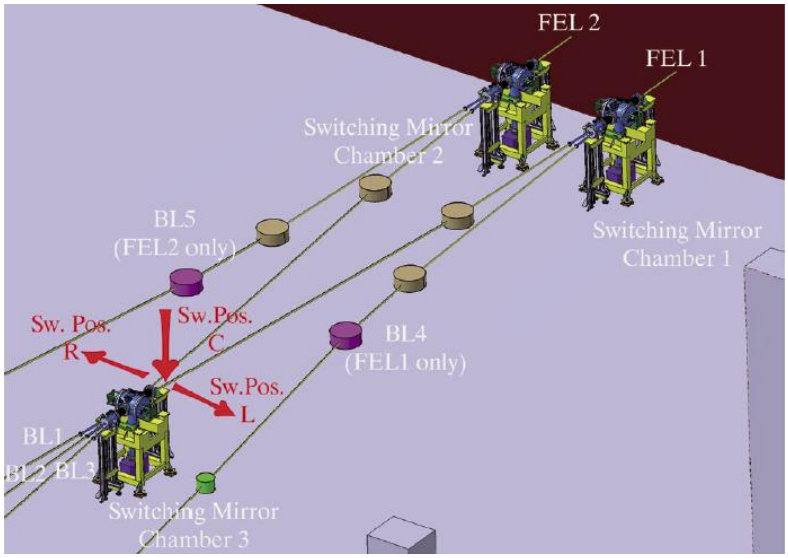

Figure 3.7 Beam transport system and Switching mirror

In order to cope with the high energy density of the beam (up to 10GW) the photon-beam transport optics is designed to operate at extremely small incident angles. The entire system is in vacuum so that no windows are needed. The main goal of the light transport system is to preserve the main properties of the light, i.e., the pulse duration, the bandwidth and the energy resolution, while transporting the light to the experimental chamber. The key element in the Experimental hall is the Switch Mirror Chamber. The main task of this element is to redirect the FEL radiation to the experimental beamlines. There are currently five experimental lines designed to be hosted in the experimental hall. Experimental stations [17] for coherent diffraction imaging (DIPROI), [22] absorption and elastic scattering from materials under extreme conditions (EIS-TIMEX), gas phase and cluster spectroscopy (LDM) are under commissioning, while additional facilities for inelastic and transient grating

spectroscopy (EIS-TIMER) and terahertz applications (TERAFERMI) are under development.

4. INTERPLAY BETWEEN THE ELECTRON LONGITUDINAL PHASE SPACE AND THE SEED LASER

4.1 Seed laser chirp

Unlike theoretical infinite waves, finite duration light pulses are not composed of a single frequency. Instead they have a frequency variation along the pulse. In our case we will be working with very short light pulses, where a single pulse is composed of many spectral components around the central frequency. Variation of frequency along the pulse is called 'chirp', analogous with bird chirping where birds emit short sound signals where the frequency also varies within a signal. Depending on the way the frequency varies along the pulse we can distinguish different chirps. In this thesis we will be dealing with linear frequency chirps and the following convention will be used for characterization: for pulse frequency increasing with time the pulse has a positive chirp, while for pulse frequency decreasing with time, it has a negative chirp

A laser pulse can have a positive or negative chirp for several reasons and the most common ones are [14]:

Natural dispersion: Dispersion is an effect that occurs when a short pulse travels through dispersive media causing different frequency components of a pulse to travel with different velocities. Since the source of the seed laser is not contained within the vacuum chamber of the accelerator, the beam travels through dispersive media like air and glass. These media induce a slight positive dispersion leading to a positive frequency chirp.

Self-phase modulation: is a consequence of optical Kerr effect [23]. The propagation of a Gaussian pulse through a medium creates a time varying refractive index, which leads to a frequency chirp along the pulse.

Compressor stage: is a process for compressing chirped laser pulses. Schematic view of the compressor stage can be seen in fig. 4.1. The incident light travels through two transmission grating dispersing the light. After dispersion, the light is reflected by a

mirror and sent through the gratings to spatially recombine. The angles and distances between the gratings and the mirror are set in such way that longer wavelengths do a longer path than the short ones.

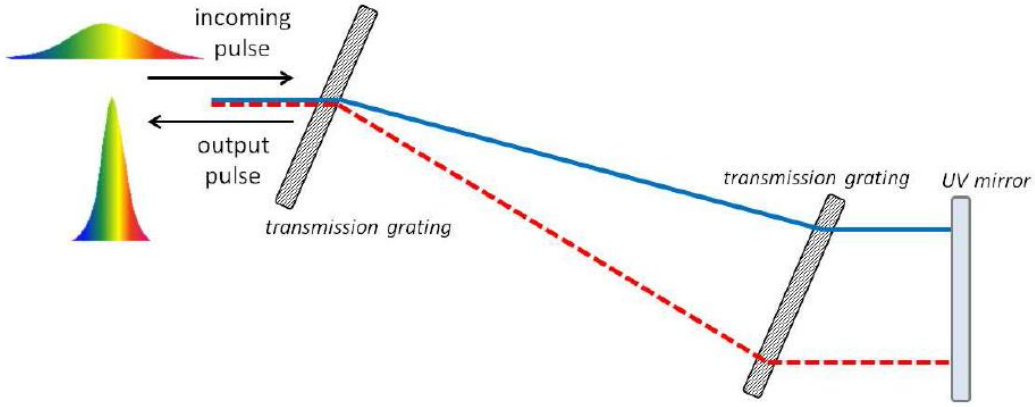

Figure 4.1 Scheme of a chirped pulse compressor [14]

The result is beam compression to its minimal duration i.e. the Fourier limit and compensation of positive dispersion. If the pulse is over compensated a negatively chirped pulse may be generated.

Here we study the phenomena of laser frequency [24] chirp. A frequency chirped electric pulse can be written as:

$$E(\omega) \propto e^{-\frac{1}{4}(\alpha+i\beta)\omega^2} \approx e^{-\frac{\omega^2}{4\Gamma}} \tag{4.1}$$

Where α and β are constant parameters. α is the parameter controlling the bandwidth of the seed laser while β is the parameter controlling its duration. The parameter Γ is defined as:

$$\Gamma = \frac{\alpha}{\alpha^2+\beta^2} - i\frac{\beta}{\alpha^2+\beta^2} = \Gamma_R + i\Gamma_I. \tag{4.2}$$

Now the Fourier transform of eq. (4.1) reads:

$$E(t) \propto e^{-\Gamma t^2} = e^{-\Gamma_R t^2 - i\Gamma_I t^2}. \tag{4.3}$$

Where

$$\varphi(t) = \Gamma_I t^2 \ . \tag{4.4}$$

If we define the time-dependent phase of the pulse, the instantaneous frequency, along the pulse reads

$$-\frac{d\varphi(t)}{dt} = -2\Gamma_I t = \omega(t) - \omega_0 \ , \tag{4.5}$$

where ω_0 is the central pulse frequency.

If the intensity is $I(t) \propto |E(t)|^2$, one finds that the rms pulse duration σ_t, in the presence of non zero chirp is,

$$\sigma_t = \frac{1}{\sqrt{2\,\Gamma_R}} = \sqrt{\frac{\alpha^2+\beta^2}{2\,\alpha}} \ . \tag{4.6}$$

Since our measurements of pulse length are presented in FWHM also noted as Δt, we used the following relation,

$$\Delta t = 2\sqrt{\ln 2}\,\sigma_t . \tag{4.7}$$

Where σ_t is the standard deviation of the bunch length, and Δt is the measured (FWHM) pulse duration.

In our experiment, we will vary the chirp of the seed laser pulse. Assuming that α is constant; let us first of all determine the relation between the laser pulse duration and the chirp. To obtain this expression, we reversed the equation (4.6) in order to obtain:

$$|\beta(\sigma_t)| = \sqrt{2{\sigma_t}^2\alpha - \alpha^2} \ . \tag{4.8}$$

By inserting the eq. (4.8) in the part presenting Γ_I in eq. (4.2) gives us the expression for the final laser chirp:

$$\Gamma_I = \mp\frac{\sqrt{2\sigma_t\alpha-\alpha^2}}{2\sigma_t\alpha} . \tag{4.9}$$

From the transformation in eq.4.7 we can also obtain an expression for standard pulse duration,

$$\sigma_t = \frac{\Delta t}{2\sqrt{\ln 2}}. \tag{4.10}$$

The equation (4.9) has two solutions for each pulse duration representing positive and negative chirp. Figure 4.2 shows the behavior of Γ_I, for multiple values of , as defined in equation (4.11) where σ_ω is the bandwidth of the seed laser:

$$\alpha = \frac{2}{{\sigma_\omega}^2}. \tag{4.11}$$

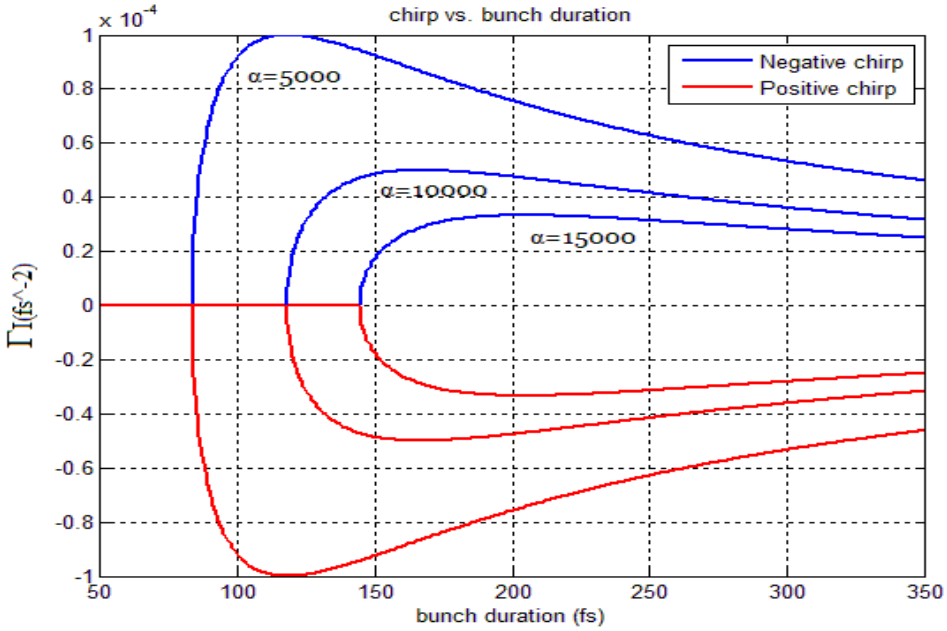

Figure 4.2 Plot of Seed laser chirp as a function of FWHM bunch duration, multiple curves are plotted with multiple seed spectral coefficients α

As seen in fig.4.2 parameter α connected to the bandwidth of the seed varies the shape of the function. In the case of seed laser used in the experiment at FERMI the bandwidth of the seed was assumed to be constant while the chirp was varied by changing pulse duration and guiding the light through some dispersive media.

4.2 Electron energy chirp

When we are considering a beam of particles instead of a single particle, it is impractical to perform calculations for every single particle. Therefore we use a representation of the whole beam. This is done by observing the particle dynamics in phase space, each particle in phase space is represented by six coordinates, four of them represent the transverse particle motion orthogonal to the coordinate along the trajectory. In this thesis we are not considering the transverse beam properties, and we are focusing only on the longitudinal phase space and its effect on the final FEL performance. Longitudinal phase space is a bi-dimensional space, in which each particle in the bunch can be described with two coordinates (z, E), representing respectively the internal longitudinal coordinate along the bunch and its energy. Several elements along the linac contribute in defining the final longitudinal phase space. The first one is represented by the RF accelerating sections [25]. When electrons with initial energy E_i enter an RF section, the resulting energy of electrons once they leave the accelerating section is,

$$E(t) = E_i + e\,V_{RF}\,\cos(\omega_{RF}t + \varphi_{RF}). \tag{4.12}$$

Where e is the electron charge, ω_{RF} and V_{RF} are respectively the RF frequency and the voltage of the accelerating structure, φ_{RF} is the RF phase of the field. We assume that on crest acceleration occurs at φ_{RF}=0 and in general all the RF sections are tuned very close to this value. Since the electron bunch has a finite temporal duration, each particle will sample a different phase and the energy-time dependence will present a negative quadratic curvature, determined by the shape of the cosine like accelerating field. In the case of off-crest acceleration we obtain a more linearized profile as seen in figure 4.3.

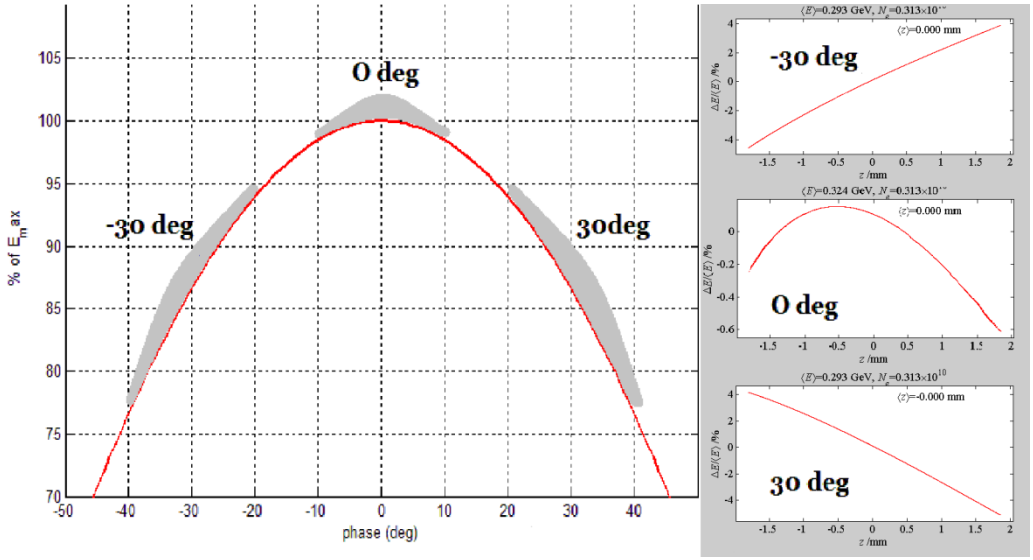

Figure 4.3 Representation of different phase accelerations using RF wave, (right) resulting longitudinal phase space shapes of different phase acceleration are shown, top to bottom -30deg , 0(on crest) and 30 deg acceleration on the left part of the figure, the acceleration process is represented with the electron bunch position (grey) on the RF wave (red).

A second contribution comes from the bunch compressor. In fact an important requirement for high power FEL emission is the production of high current electron bunch and this means that [14] the electron bunch must be longitudinally compressed. A typical way to compress the electron beam consists in imposing an energy correlation along the bunch by setting off-crest some of RF sections and sending then the beam through a magnetic chicane, called bunch compressor. In this latter, an electron with an energy difference ΔE with respect to the energy E_0 of the reference particle, travels along a different path. This results at the end of the chicane in a spatial displacement Δz, given by the following equation:

$$\Delta z = R_{56}\frac{\Delta E}{E_0} + T_{566}\left(\frac{\Delta E}{E_0}\right)^2, \tag{4.13}$$

where R_{56} and T_{566} are the first and the second order dispersion coefficients [21]. However in order to linearly compress the electron bunch it is necessary to compensate the non linearity of the RF curvature and of the second order dispersion term T_{566}. At this purpose a high harmonic cavity is usually adopted by operating it in decelerating mode, providing the necessary compensating non linear term to the longitudinal phase space. A final contribution to the longitudinal phase space comes

from the longitudinal wakefields generated in the linac structures during the beam passage. Moreover, when the bunch is shortened, the effects of the wakefields in the downstream linac become important and strongly contribute in defining the final longitudinal phase space. Figure 4.4 shows an example of the final longitudinal phase space measured at the end of the FERMI linac.

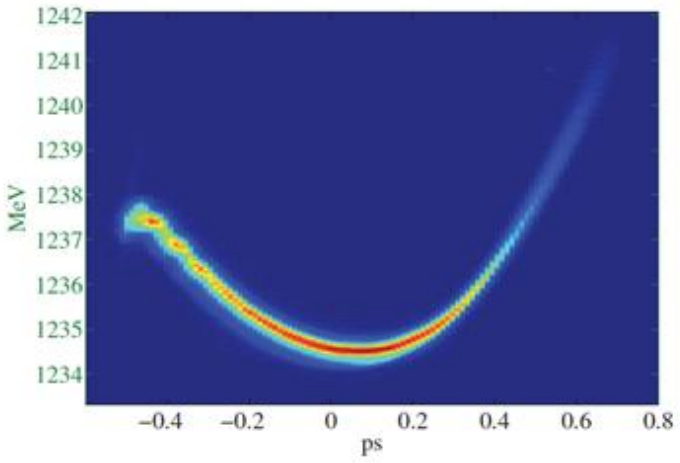

Figure 4.4 An example of electron longitudinal phase space measured at the end of the FERMI linac [26]

As one can observe from the figure 4.4, the longitudinal phase space can be fitted by a third order polynomial having the following expression

$$E(z) = E_0 + \chi_1 z + \chi_2 z^2 + \chi_3 z^3. \quad (4.14)$$

Where z is the coordinate along the bunch, E_0 is the nominal energy of the beam χ_1, χ_2 and χ_3 are the linear, quadratic and cubic coefficients. This will become especially important in the following sections where measurements and characterization of longitudinal phase space will be explained.

4.2.1 Measurement of longitudinal phase space

At FERMI@elettra the measurement of the electron beam energy distribution [26] can be performed at various positions along the accelerator. In our experiment we have used the energy spectrometer placed at the end of the linac, called Diagnostic Beam Dump (DBD) and a high energy radio frequency deflector (named HERFD

[27]). The RF field inside the HERFD cavity provides a force in the vertical direction that is proportional to the electric field as.

$$F_{\perp}(z) = e\,E_0 \sin(k_{RF} z + \varphi_{RF}). \quad (4.15)$$

The phase of the RF wave with respect to the electron bunch, is set to place the center of the bunch at $\varphi_{RF}=0$, providing an upwards kick to the electrons in the head of the bunch and a downwards one in the tail as seen in figure 4.5:

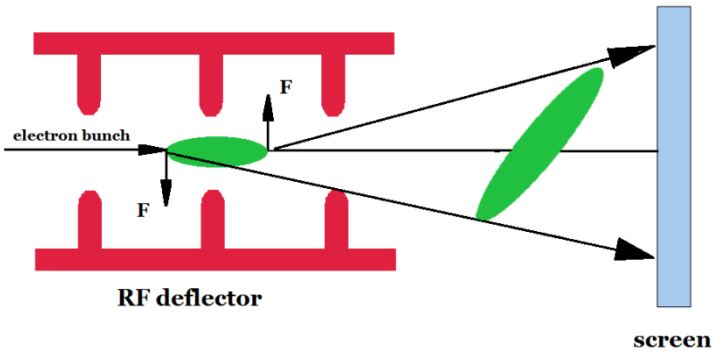

Figure 4.5 Schematic view of RF deflector cavity operation [27].

This force than translates the longitudinal beam characteristics in the vertical direction so that, by calculating the relation between the transverse beam size observed at the screen we can obtain information about the duration of the bunch. Using the deflector HERFD in combination with the spectrometer that disperses the electrons in the horizontal plane according to their energy, allows to reconstruct the beam longitudinal phase space, by imaging the beam on a downstream screen.

The obtained beam image on the screen allows us to distinguish the temporal and energy distribution along the bunch. There are many important information that were extracted from these images, the two main profiles are the energy and the current profile

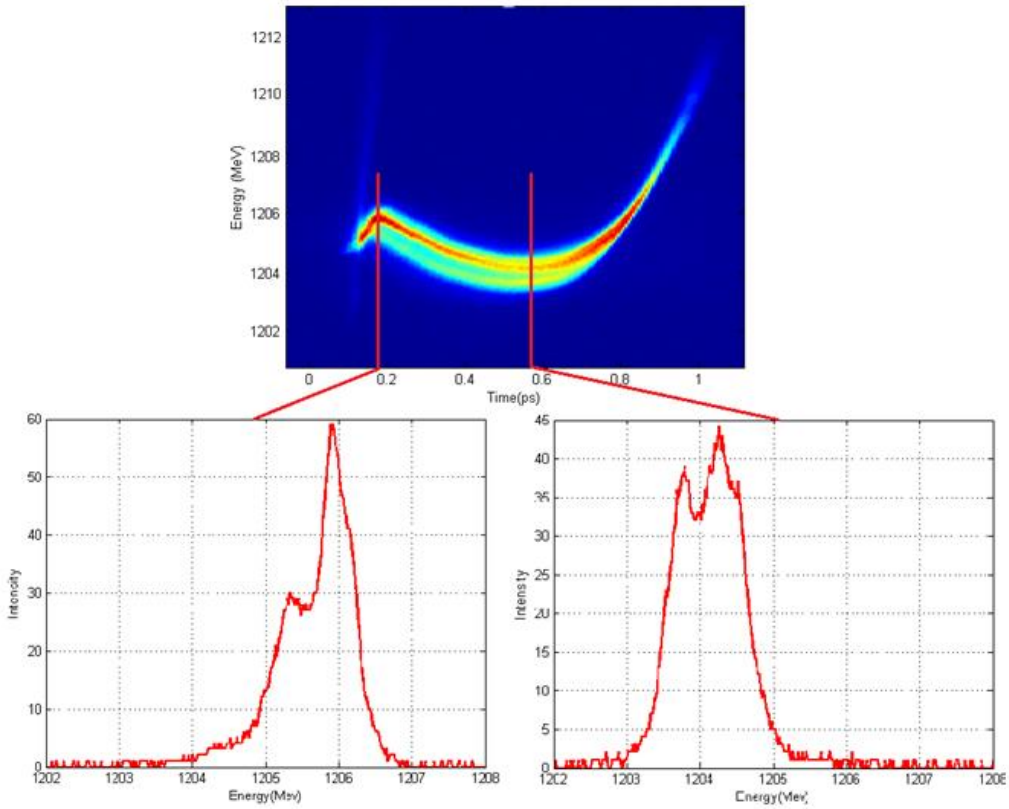

Figure 4.6 Measurement of longitudinal phase space at the end of linear accelerator at FERMI@elettra, top raw spectrometer image, bottom slice energy spread.

Fig 4.6 shows the raw image from the screen of the beam diagnostic spectrometer (top). The vertical axis represents the electrons energy while horizontal axis represents time (i.e., position) along the bunch. By slicing the profile along the x axis as shown in fig. 4.6 one can obtain the time sliced energy profiles (bottom two plots) and therefore can evaluate the time slice energy (mean) and energy spread (width) along the bunch. Moreover the beam current profile can be measured by integrating each time-sliced energy profile along the bunch.

Fig. 4.7 shows the time-sliced energy (on the left) and current distribution (on the right) obtained in a typical machine configuration. From the energy distribution along the bunch one can clearly see the previously mentioned quadratic shape described by the equation 4.14. One can also see that the curvature of energy profile is increasing from head towards the tail. The increase in curvature will be shown in the later sections where we will characterize this curvature by fitting the energy profile with a local second order polynomial. The characterization along with the calculation of quantities connected to energy profile will be presented in section 5.2.

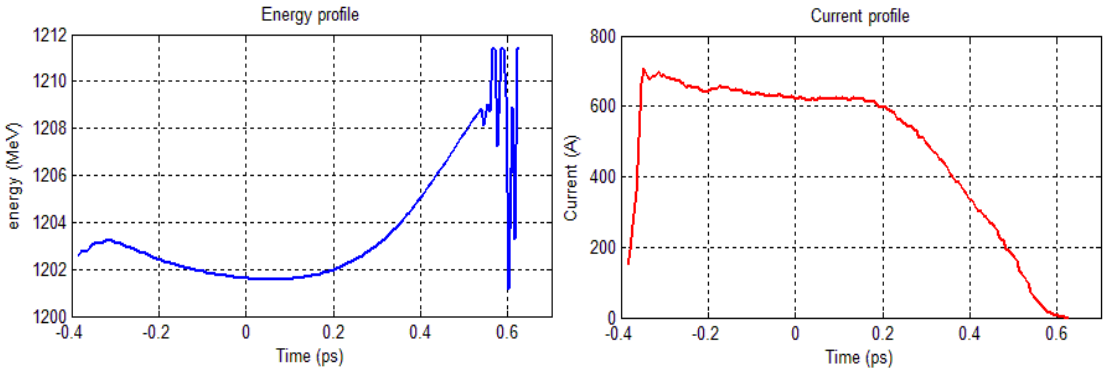

Figure 4.7 Examples of longitudinal phase space energy and current profile.

From the current profile we can obtain information about how the electron content characterizes the bunch. Fig.4.7 shows that the main part of the bunch, holding most of the charge content is around 0.6 ps long (from -0.3 ps to 0.3 ps): the current in this part of the bunch is almost constantly over 600 A. Since the electron bunch at the injector exit has about 60 A of peak current, the beam has been compressed by a factor 10 along the linac.

These are the actual data taken at the day of the experiment carried out to see the interplay between the electron longitudinal phase space and the seed laser frequency.

4.3 Chirp compensation

As has been mentioned in the previous chapters, [28] in a seeded high-gain FEL an external seed laser is made interacting with the relativistic electron beam to initiate the process. FEL radiated wavelength is defined by eq. (4.16), in our case parameters λ_u (undulator period) and K (strength of unduator magnetic field) are constant since we did not change the undulator settings during the experiment. So in order to obtain a certain wavelength one should set the beam at a certain energy (γ is the relativistic coefficient connected to electron energy).

$$\lambda_R = \frac{\lambda_U}{2\gamma^2}\left(1 + \frac{1}{2}K^2\right) \tag{4.16}$$

Since we have seen that energy of our beam has a curvature one cannot generate a transform limited FEL pulse with an un-chirped laser. Thus the energy curvature could be compensated by using a proper seed laser chirp. Here we do not face the theoretical study of the interplay between the electron energy chirp and the seed laser frequency chirp and we refer to already published articles, for more details [28], [29], [30] and [31]. Here we use the results of those studies.

Following from eq. 4.14, we can define the electron energy chirp as [32]:

$$\frac{dE(z)}{dz} = \chi_1 + 2\chi_2 z + 3\chi_3 z^2. \tag{4.17}$$

We will only consider linear and quadratic terms due to local analysis of the beam properties explained in chapter 5. If combined with a dispersion factor R_{56} the energy chirp generates the compression factor

$$C(z) = \frac{1}{1+\frac{R_{56}}{E_0}\frac{dE(z)}{dz}} = \frac{1}{1+\frac{R_{56}}{E_0}\chi_1+\frac{R_{56}}{E_0}2\chi_2 z}. \tag{4.18}$$

R_{56} is the strength of dispersive section and E_0 is the mean energy of the electrons. The energy modulation imposed by the seed laser at a frequency ω_0 is consequently compressed by the same factor C of equation 4.18. The resulting frequency of the bunching after energy modulation of the beam reads,

$$\omega_{ins}(z) = \omega_0 C(z) = \frac{\omega_0}{1+\frac{R_{56}}{E_0}\chi_1+\frac{R_{56}}{E_0}2\chi_2 z}. \tag{4.19}$$

After applying the relation z = -t c, the Taylor expansion around t=0 gives,

$$\omega_{ins}(t) = \frac{\omega_0}{1+\frac{R_{56}}{E_0}\chi_1} + \frac{2R_{56}\omega_0 c}{E_0\left(1+\frac{R_{56}}{E_0}\chi_1\right)^2}\chi_2 t = \omega_{FEL} + 2\xi t \tag{4.20}$$

Where

$$\omega_{FEL} = \frac{\omega_0}{1+\frac{R_{56}}{E_0}\chi_1}, \tag{4.21}$$

$$\xi = -\frac{{\omega_{FEL}}^2}{\omega_0}\frac{R_{56}c}{E_0}\chi_2. \quad (4.22)$$

ω_{FEL} is the central frequency of the FEL that is shifted with respect to the seed laser frequency if the electron bunch has a linear chirp in the energy distribution. The term ξ represents the FEL frequency chirp that depends on the quadratic chirp χ_2 in the electron energy distribution.

In order to compensate this frequency chirp in the FEL output we need to generate a seed laser with a frequency chirp Γ_I equal to the term ξ of the equation 4.22. We have performed a series of experiments, described in the next chapters, with different seed laser frequency chirps and we have measured the effect on the FEL spectra.

5 DATA ANALYSIS

5.1 Alignment of longitudinal phase space and FEL emission data

In our experiment we have used the energy spectrometer placed at the end of the linac, called Diagnostic Beam Dump to perform the measurement of longitudinal phase space as described in section 4.2.1. The time scale was therefore obtained by deflecting the beam and translating longitudinal position into vertical displacement using a HERFD deflection cavity. We also measured the FEL emission intensity and spectra versus the longitudinal position of seed laser on the electron beam.

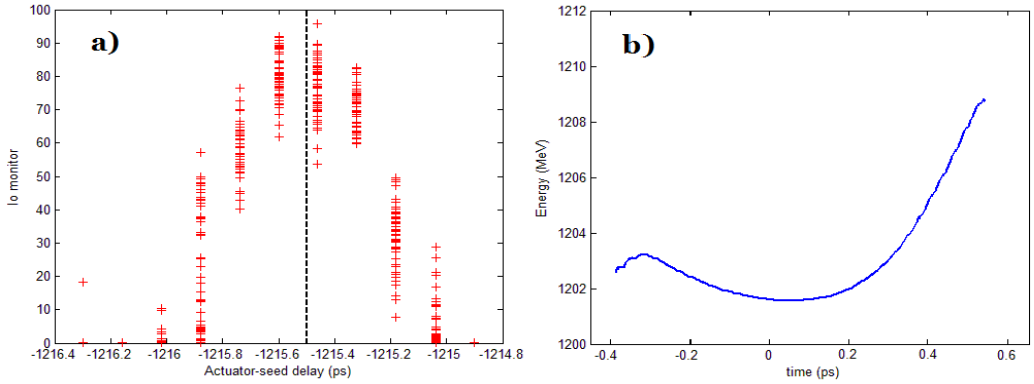

Figure 5.1 a) IO-monitor/Actuator-seed delay (obtained by measuring FEL emission) each point corresponds to one measurement there were 50 measurements performed for each seed delay position. b) Energy of electrons/ time (measured at the end of linac).

In order to see the interplay between the measured quantities one has to know on what part of the bunch was placed the seed pulse when a given spectra was acquired. This information was obtained by analyzing the shape of the bunch and its energy profile. The time scale on the energy profile (fig.5.1 b) is our reference, t=0 is set to be in the center of the bunch, negative time values correspond to the head of the bunch while positive ones correspond to the tail. Fig 5.1 a) represents the ionization monitor or gas absorption measurement of FEL intensity. This is a noninvasive measurement, which means it could be performed at the same time of the spectra

acquisition, resulting in the same horizontal axis intervals and seed delay positions as the spectral measurements. What needed to be done is to find out which value of the seed delay (fig 5.1 a) corresponds to which position in time on the energy profile. We know that if the seed laser is not positioned on the electron bunch the FEL intensity will be zero since we do not have the process of harmonic generation. In order to make a more precise alignment we calculated the centroid position (dashed line in fig 5.1 a)) of the ionization monitor vs. seed delay position. Aligning the centroid position with time t=0, has allowed us to know where on the bunch the seed laser was positioned when a certain measurement was taken.

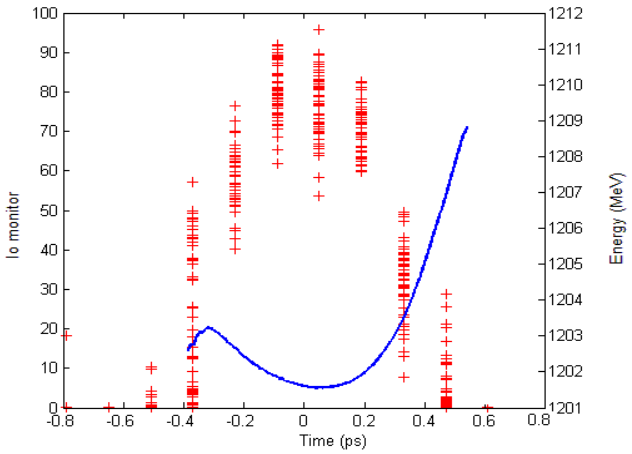

Figure 5.2 Aligned IO monitor and Electron energy from fig.3.1

Fig 5.2 shows an example of the resulting alignment.

5.2 Calculation of the electron chirp

As anticipated in chapter 4.2 the energy of electrons along the bunch can be well fitted by a third order polynomial (see equation 4.14). This means that the quadratic term χ_2, that is responsible of the frequency chirp in the FEL radiation output, varies along the bunch. So we have performed a second order polynomial fitting around each temporal slice, in order to obtain the linear and the quadratic terms all along the bunch. For convenience we apply the following variable change t=-z/c, so the local quadratic fitting becomes:

$$E_j(t) = E_{j,0} - (c\,\chi_{1,j})\,t + (c^2\chi_{2,j})t^2, \qquad (5.1)$$

where the subfix "j" indicates the slice around which we perform the fitting, $Ej_{,0}$ is the local central energy of electrons at slice j. The temporal interval for the fitting is about 200fs and corresponds approximately to the seed laser pulse length. . Figure 5.3 reports the results of the local second order polynomial fitting of eq. 5.1, showing the behavior of the slice linear and quadratic coefficients along the bunch, together with the slice mean energy. From the coefficients of the locally fitted function we will be able to calculate both of the main parameters, central wavelength defined in eq.4.21 and the ξ of the seed laser that would compensate for the energy curvature, calculated by using eq.4.22 (section 4.3).

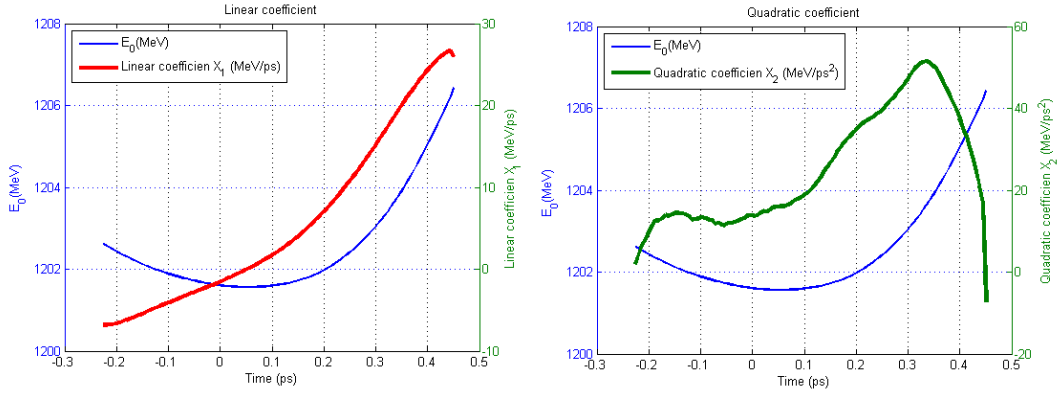

Figure 5.3 Behavior of the slice energy (blue line) and of the slice linear coefficient (red line) along the bunch.

Six sections were chosen at an interval approximately equal to the rms width of the seed pulse. The local values of the coefficients and the resulting ξ at the positions presented in fig.5.4 are reported in table 5.1.

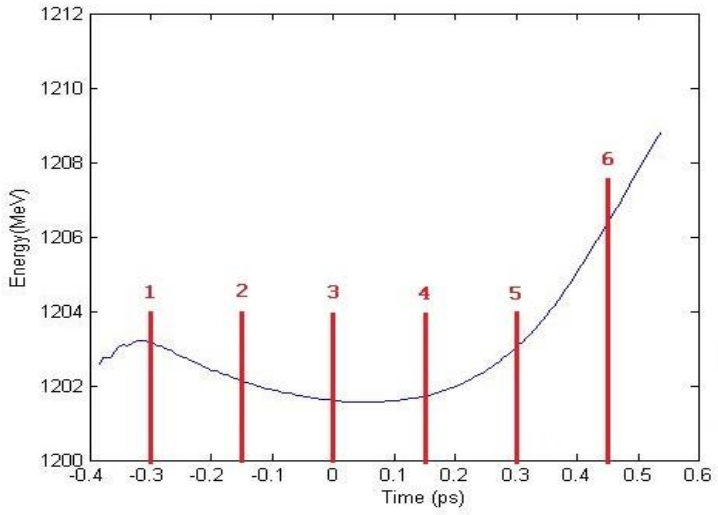

Figure 5.4 Locations of the six sections on the energy profile.

Section	*Section 1 t=-0.3ps*	*Section 2 t=-0.15ps*	*Section 3 t=0ps*	*Section 4 t=0.15ps*	*Section 5 t=0.3ps*	*Section 6 t=0.45ps*
Coefficient $c^2\chi_2$	-88.7	14.4	14.3	26.2	47.9	19.0
ξ (fs^{-2})	0.824*e-04	-0.134*e-04	-0.133*e-04	-0.243 *e-04	-0.445*e-04	-0.176*e-04
Std of ξ	0.065*e-04	0.016*e-04	0.007*e-04	0.007*e-04	0.009*e-04	0.054*e-04

Table 5.1 Values of the quadratic fit coefficients and chirp in six sections

By observing the coefficients in table 5.1 it is clear that the curvature of the electron profile changes rapidly along the bunch, resulting in big changes of the calculated ξ. In sections where the value of ξ from the table is close to the value of the seed chirp Γ_I we expect a decrease of the FEL bandwidth.

The fig. 5.5 shows the distribution of ξ needed to compensate the electron energy chirp. The distribution was calculated using the quadratic fit coefficient presented in fig. 5.3

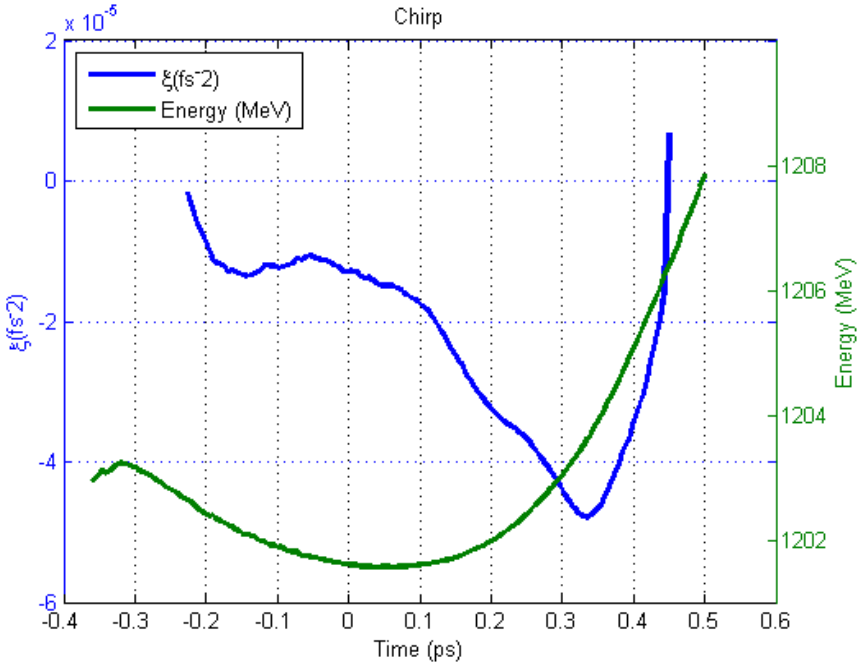

Figure 5.5 Plot of seed Γ needed as a continuous function.

For this experiment, the sixth harmonic of the seed wavelength was generated, resulting in the final wavelength of 43.5nm. The calculated prediction for the central wavelength is presented in fig. 5.8

5.3 Experimental results

During our measurements FERMI was setup to operate at 1198MeV on the FEL-1 undulator line. APPLE II undulators were set up to provide circular polarization at a wavelength of 43.5nm which is the sixth harmonic of the seed laser wavelength. It has been previously seen in section 5.1 and in fig.5.1 a), that the measurements of FEL emission were done by steps. We considered 11 seed delay positions along the beam, those positions were arranged similarly to the sections in fig 5.4. Raw image of such scan is presented in fig. 5.6: every 50 shots the seed delay temporal position was changed, sampling a different portion of the electron bunch with its own χ_1 and χ_2 and therefore resulting in a FEL emission with a different wavelength (vertical axis of fig. 5.6) and spectra. An example of FEL spectrum (fig.5.6, bottom) for a particular seed laser position and the corresponding Gaussian fitting performed to

evaluate the peak position (i.e. ω_{FEL}) and its spectral bandwidth is shown in bottom fig.5.6.

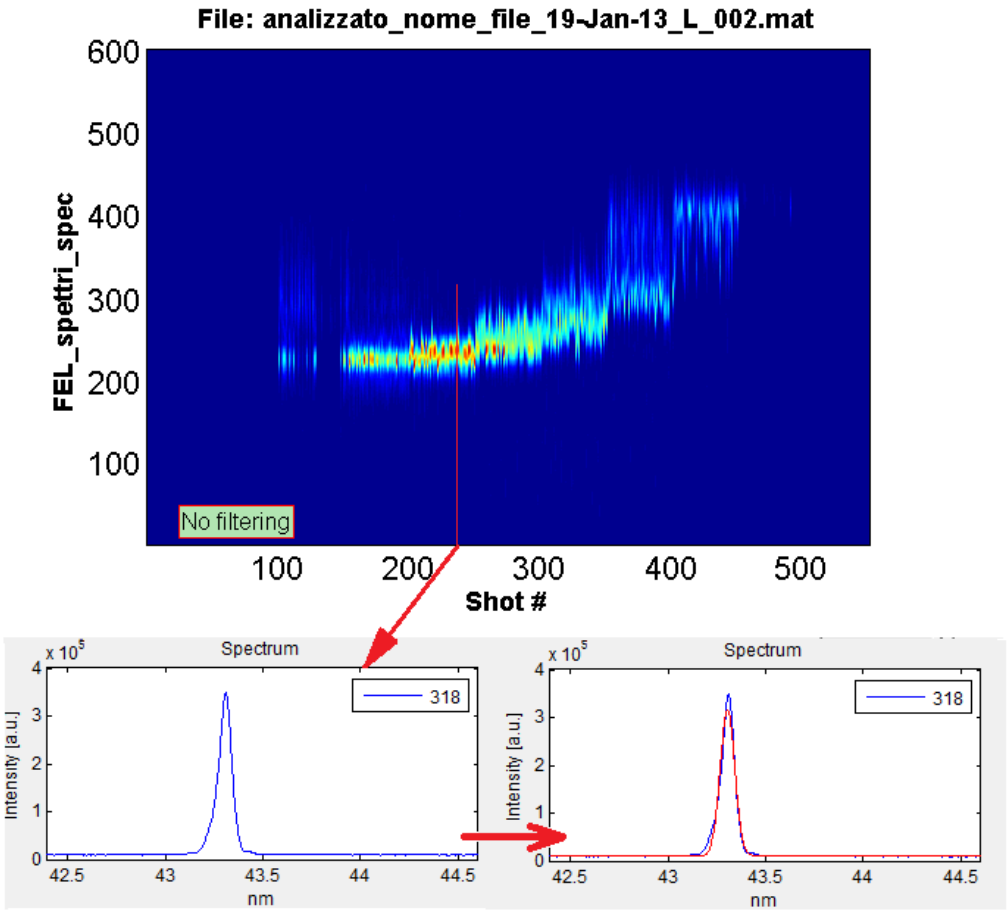

Figure 5.6 Fitting a spectra using Gaussian function, operation of matlab code.

In the post-processing of the raw data we have selected some spectra and disregarded other ones because the latter were affected by significant noise. Noisy spectra can occur due to jitter of several machine parameters such as the energy of electrons, current fluctuations and the position of seed with respect to electron bunch. Non-Gaussian shapes could also be caused by bunching instabilities, causing multiple spectral peaks or overbunching.

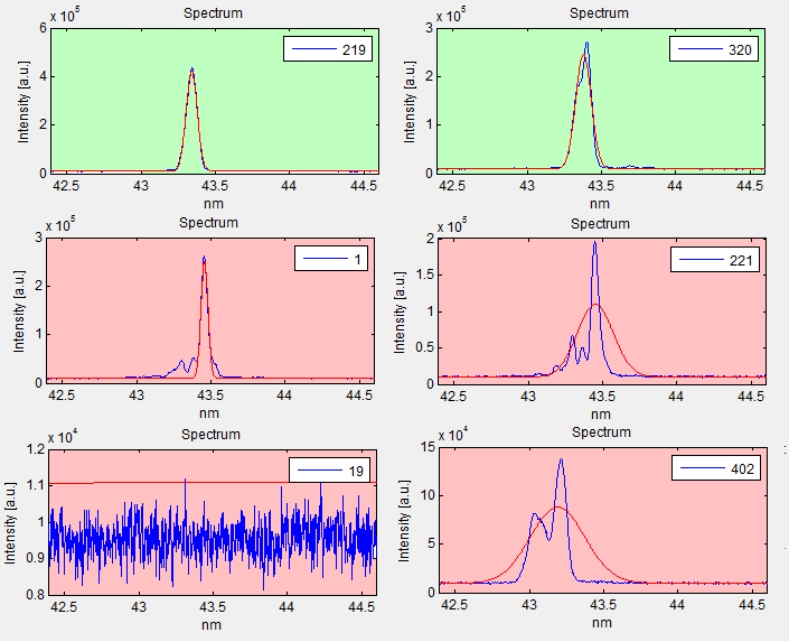

Figure 5.7 Examples of disregarded spectra (red) and acceptable spectra (green)

An example of the analysis we carried out is shown in figure 5.7. The green background spectral images were accepted, while red ones are examples of what was disregarded. Bottom left image is an example of spectra when, (due to jitter) the seed was not placed on the electron bunch thus only noisy spontaneous emissions were acquired. Spectra 1 and 221 in fig.5.7 are examples of what was found in the analysis of some measurements where FEL emission was very unstable, as will be presented in following sections. In particular, during the analysis an interesting phenomenon was found. At some seed positions, for the measurements when a negatively chirped seed pulse was used, double or multiple peak spectra like that of plot 402 on fig.5.7, were found. Due to the non-Gaussian shape of these spectra no spectral information could be extracted from these fits, resulting in a gap in the plot of σ_{FEL}. For the positive chirp seed there was a broadening of spectra at approximately the same position, but in general there were no double peaks and noisy spectra, presenting unstable emission. This phenomena will be investigated in details in next future experiments.

Once useful spectra were extracted, they were analyzed by a home-made software. Our main interest was in the spectral width, intensity and central wavelength of FEL emission.

We have performed experimental measurements of the FEL intensity and spectra by setting the seed laser in three configurations: with a negative frequency chirp, with a positive one and with an almost zero chirp.

As discussed in chapter 4, the central wavelength of FEL emission ω_{FEL} depends on the linear coefficient χ_1 of the electron energy-time dependence (see eq.4.21)

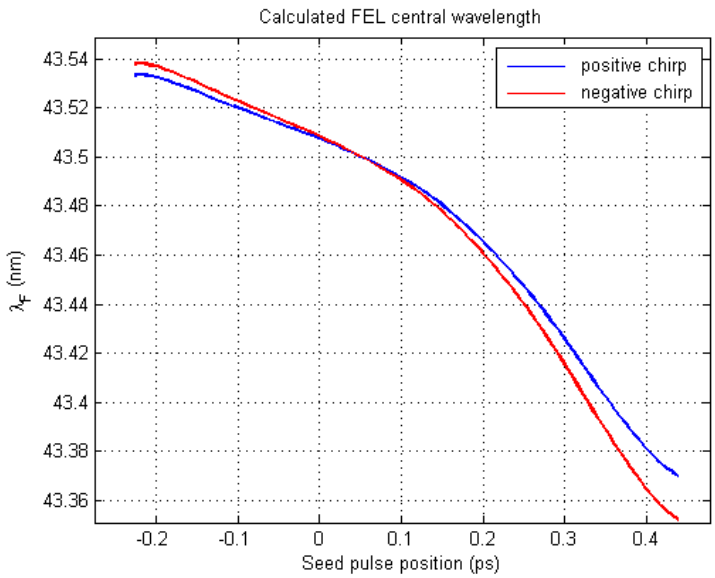

Figure 5.8 ω_{FEL} for negative seed chirp (red) and positive seed chirp (blue)

Fig.5.8 shows the theoretical FEL central wavelength shift versus the seed laser position over the electron bunch in two experiments, one with a positive chirp in the seed laser frequency and one with a negative one.

When the parameter Γ_I of the seed laser and the parameter ξ defined in the previous sections, match we would expect the narrower bandwidth of FEL emission since the laser chirp should compensate for the electron energy chirp. We introduce a new parameter $\Delta\Gamma$ that is calculated as the difference between ξ and Γ_I. Thus the parameter $\Delta\Gamma$ should give an estimate of the bandwidth for a certain seed chirp: when $\Delta\Gamma$ is close to zero, one should obtain the narrower FEL bandwidth (σ_{FEL}).

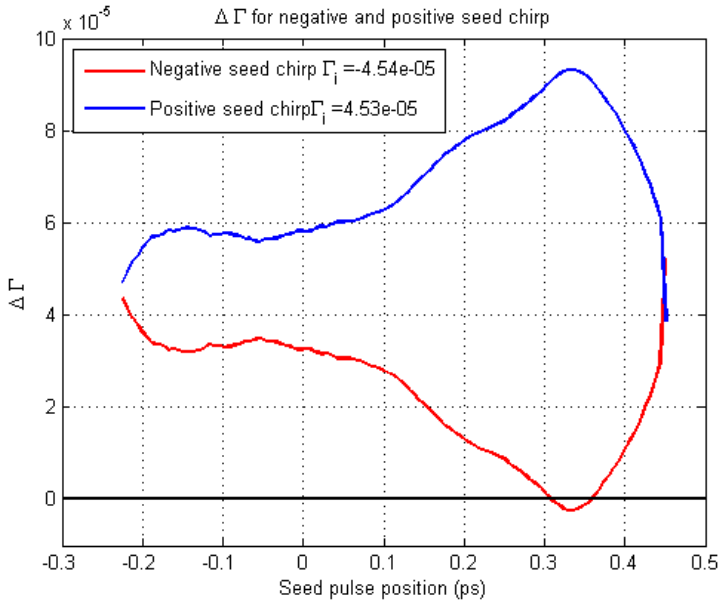

Figure 5.9 An example of $\Delta\Gamma$ for both negative (red) and positive (blue) Γ_I

An example of $\Delta\Gamma$ for both the positive and the negative seed chirp is represented in fig.5.9. We can see that for the positive seed chirp we expect an expansion of bandwidth from head to tail of the bunch, while for negative seed chirp we expect an improvement and finally almost complete compensation at around 0.3ps. $\Delta\Gamma$ will be also plotted using a green line in all figures representing the measured bandwidth σ_{FEL}. Measurements were performed by trying to keep the shape of longitudinal phase space unchanged (see section 4.2), and by varying the seed laser chirp. As we know from section 2.3.1, there are two main parameters affecting the bunching, intensity of the seed laser responsible for electron energy modulation inside the modulator, and the strength of the dispersive section responsible for turning energy modulation into spatial modulation. In the aim of keeping the bunching constant, we needed to keep the peak seed intensity constant. This was done by increasing the seed pulse energy when pulse length was increased.

During the experiment various seed laser settings were used. In order to show the main findings of our experiment three examples with different seed chirp will be presented. A positive chirp configuration with duration 197fs, a short 180fs pulse with almost zero chirp and a longer 227fs negative chirp pulse. The short pulse was used in an effort to create a seed chirp as close to zero as possible. The next sections

will provide an explanation of the experimental setup used to obtain a particular laser chirp, and show the resulting measurements of FEL spectra.

In order to be able to compare the results obtained using positive and negative chirp we needed a good temporal reference point to compare the value of σ_{FEL}. The reference point was chosen where the FEL intensity is maximized, that is within the range from -0.2ps to 0ps. This time-sliced region corresponds to the portion of the bunch with the properly tuned electron energy.

5.3.1 Zero 'natural' seed chirp

The first presented measurement will show a scan performed with seed positive chirp. In order to understand how a chirped seed pulse is created we explain the process of third harmonic generation of a Ti-Sapphire laser. The original laser has a Gaussian shape, zero chirp and a wavelength of 800nm. It is then sent through a piece of diffractive material called BBO in order to create the second harmonic with a wavelength of 400nm. Then the seed laser is passed through another piece of the same material in order to obtain the third harmonic of about 260nm. The process of passing the laser pulse through dispersive material that generates the harmonics induces a positive chirp. Finally, this positively chirped pulse was compressed using the compressor gratings in order to find the shortest possible duration. Considering that the bandwidth of the seed pulse remains unchanged a pulse generated in this way should have the smallest chirp possible. This zero chirp will also be referred to as the 'natural' chirp since this is the starting point of all the used seed configurations.

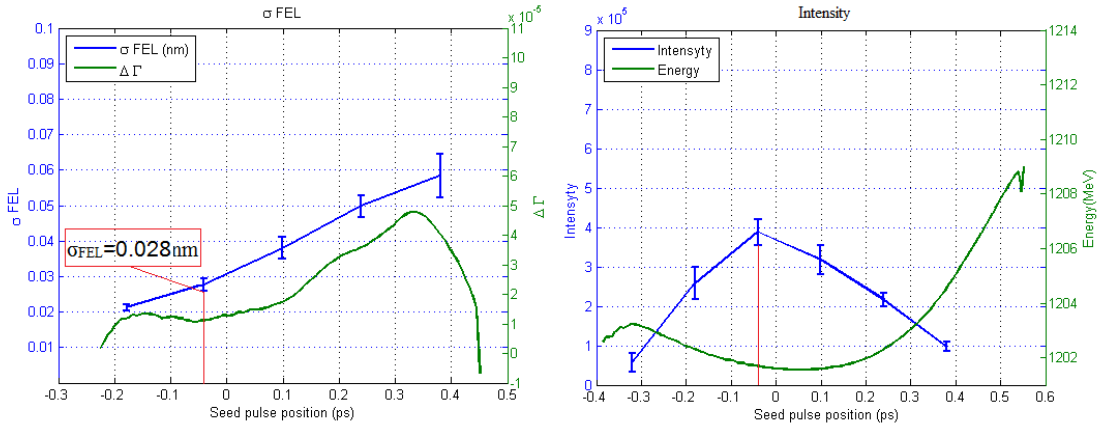

Figure 5.10 σ_{FEL} and intensity with respect to the seed pulse position

Errorbars in all figures presenting bandwidth, intensity or central frequency have the size of standard deviation of the considered data for a particular seed position. Fig.5.10 shows the selected reference point on both the intensity and σ_{FEL} plots. In the left plot the blue line represents the results of the measurement of σ_{FEL}; the green line represents $\Delta\Gamma$. It is also clear that by using this chirp we obtained very stable emission and behavior of σ_{FEL} which clearly follows the shape of $\Delta\Gamma$, so that the shortest FEL bandwidth (0.028nm) corresponds to the min value of $\Delta\Gamma$. On the right we can see the measured intensity of FEL emission, that has its maximal intensity inside the interval -0.2ps to 0ps. This indicates that the area of high FEL gain was slightly moved towards the head of the bunch. The green line (in the plot on the right of fig, 5.10) represents the energy of electrons along the bunch.

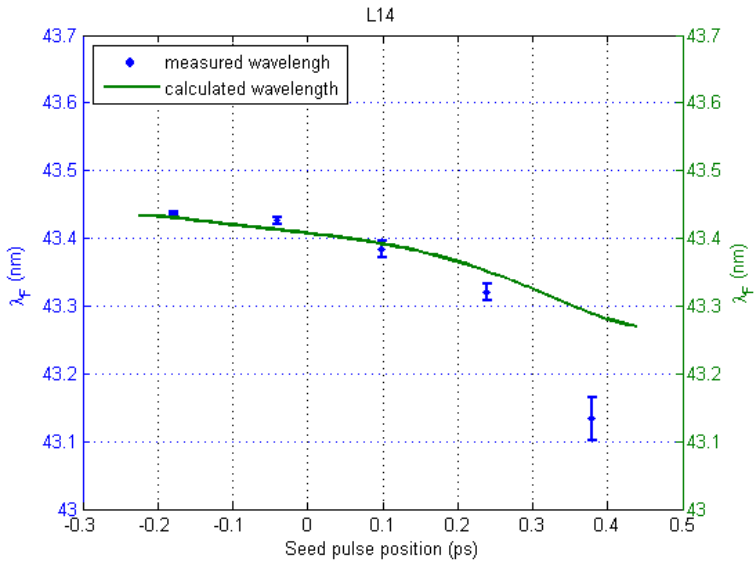

Figure 5.11 Evolution of peak position along the bunch.

Fig.5.11 shows good agreement between the calculated central emission wavelength and the actual measured central wavelength, for the 'natural' chirp measurement. We can spot that the trend of the central wavelength follows the calculated value from the head of the bunch until about 0.25ps; beyond this point the FEL intensity is too weak to be properly detected because the electron energy is too far from the optimum one and the spectra analysis provides unreliable results.

5.3.2 Positive chirp

In order to increase the positive chirp, the 'natural' seed chirp was passed through another piece of diffractive material. In our experiment we used 16mm of CaF2 crystal. CaF2 is a dispersive material that increases the chirp and also the pulse duration. The latter was increased from 180fs to 194fs. The resulting laser chirp was $\Gamma_I = +0.446\,e^{-4}fs^{-2}$. Since our electron profile had a positive energy curvature, a negatively chirped seed was required in order to compensate for this curvature. The positively chirped seed used in this example should result in broadening of the spectra across the entire range compared to zero and negative chirp.

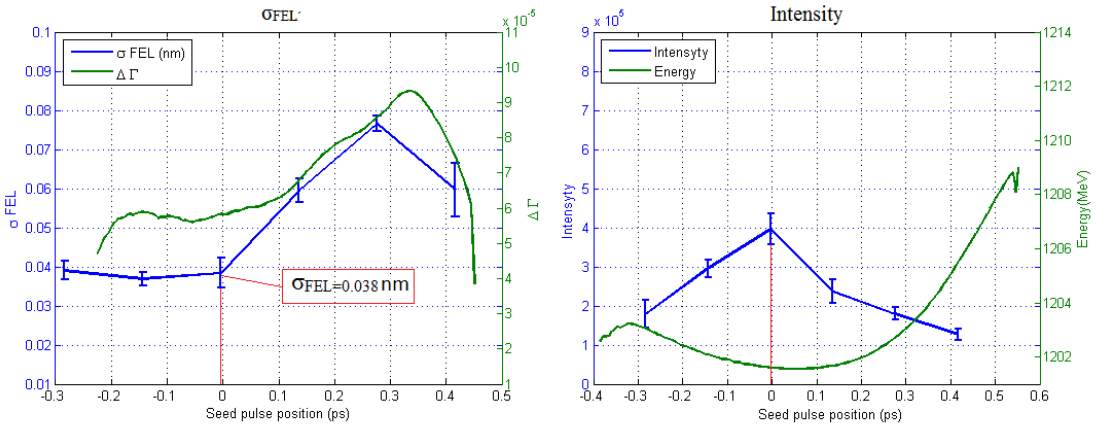

Figure 5.12 σ_{FEL} and intensity with respect to the seed pulse position

In left plot of fig.5.12 the blue line represents the results of the measurement of σ_{FEL} and green line represents $\Delta\Gamma$. Behavior of the measured bandwidth clearly follows the shape of $\Delta\Gamma$ indicating an agreement with the theoretical estimation. The min spectral bandwidth at the reference point (red line) using this seed laser chirp was 0.038nm.

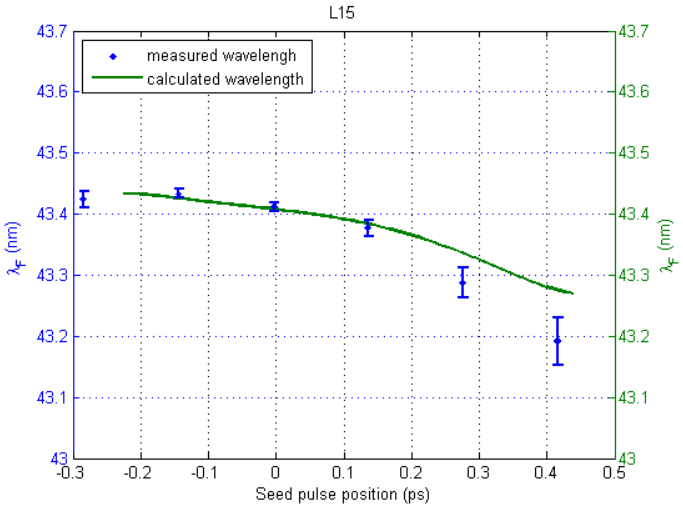

Figure 5.13 Evolution of peak position along the bunch.

Fig.5.13 again shows a comparison between the measured central wavelength and the one calculated from the shape of the energy profile. Looking at the frequency shifting along the bunch, one can see that the measured data follow tightly with the calculated estimation as long as the seed laser overlaps the beam portion with a proper energy. As in the previous case, the last temporal slice reliable is at about 0.25ps.

5.3.3 Negative seed chirp, long pulse:

The negative chirp was created using the natural positive chirp and passing it through a compressor. This device can over compress the pulse and cause that the head and the tail of the pulse to exchange their position resulting in a change in the chirp sign. A schematic view of a laser pulse compressor together with an explanation of its operation can be found in section 4.1. The seed laser in this configuration has a pulse length of about 227fs and an estimated negative chirp of $\Gamma_I = -0.4150\ e^{-4}fs^{-2}$. As in the previous cases, the maximum FEL intensity has been detected when the seed overlaps the same electron temporal slice (see fig.5.14), with an enhancement of about 30% relative to the positive chirp and "almost-zero" chirp cases.

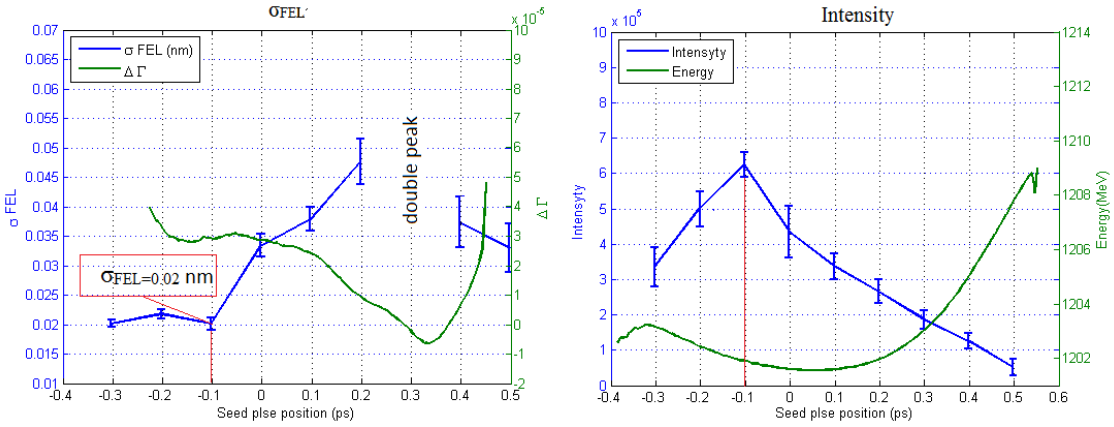

Figure 5.14 σ_{FEL} and intensity with respect to the seed pulse position

Moreover as expected the FEL bandwidth in this case assumes the minimum value of 0.02nm and this confirms that the negative chirp of the seed compensates the electron positive curvature. We observe that the best electron portion where we should measure a complete chirp compensation, (i.e. corresponding to $\Delta\Gamma=0$) , are in the positive temporal area (about 0.3-0.4ps) where electrons have an energy very far from the resonant condition. In this portion in fact spectra show double-peak structures and a poor FEL intensity. Furthermore, the longer seed laser adopted in this configuration leads to have a larger electron portion participating in the FEL process. Thus several electron temporal slices having very large and different energy quadratic chirp interfere destructively, deteriorating the output FEL spectrum.

As before the FEL central wavelength shift is measured and compared with the expectation (see fig.5.15), and a good agreement is found also in this case. Nevertheless the discrepancy observed before for seed laser timing greater than 0.25 ps, is now present already at about 0 ps. A possible interpretation of this phenomenon is again related to the use of such a larger seed laser pulse

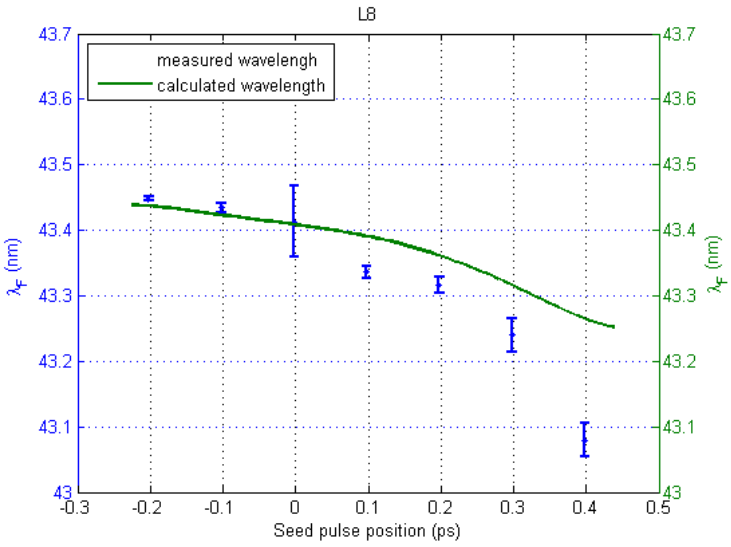

Figure 5.15 Evolution of peak position along the bunch.

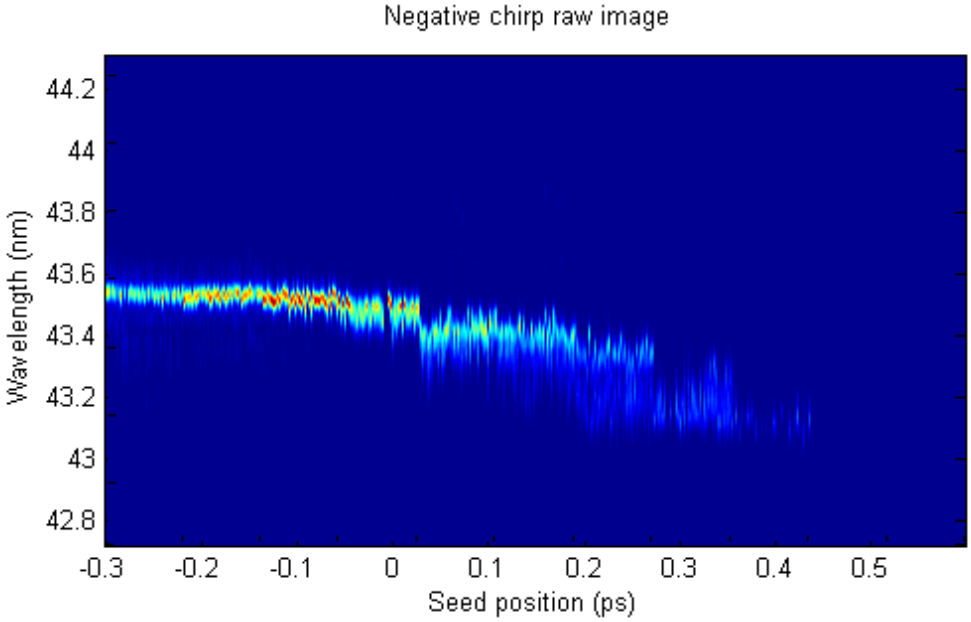

Figure 5.16 Evolution of peak position along the bunch.

CONCLUSION

In this thesis we have presented an experimental investigation of the interplay between the electron beam energy curvature and the seed laser frequency chirp and the impact on the seeded FEL performance. Experiments were carried on at the FERMI HGHG FEL, in particular on the FEL-1 line, by setting the machine to lase at 43.5nm. The energy curvature of the electron beam has been measured, performing a time-sliced second order polynomial fitting along the bunch to obtain the local linear and quadratic coefficients that are responsible respectively for a shift and a spectral broadening of the FEL output radiation in case of a un-chirped seed laser. We have therefore studied the possibility to compensate the electron energy curvature by properly setting a frequency chirp to the seed laser. Since the electron second order energy chirp is positive and increased from the head to the tail of the bunch, in case of a positive seed laser frequency chirp no compensation occurred. By the way scanning the seed delay in order to make it overlaps different regions of the bunch, from the head to the tail, we observed as expected an increasing broadening of the FEL spectrum. The minimum FEL bandwidth we measured was about 0.038 nm, which is larger than what we measured for a "quasi-zero" chirped seed laser (0.028 nm). The undulator were set to be resonant at an electron energy corresponding to a longitudinal bunch portion close to the head, so when the seed overlaps this region the FEL intensity was maximized and we consider the FEL bandwidth measured in this condition. When the seed has been prepared with a negative frequency chirp and the seed laser overlaps the resonant electron bunch portion, the FEL was 30% more intense than in the previous cases and with a bandwidth reduced to 0.02 nm. This confirms the possibility to compensate the energy curvature of the electron beam with a proper negative frequency chirped seed laser.

However we observed in the negative chirped case that when the seed overlaps other longitudinal portion the FEL spectrum was deteriorated. Despite this phenomena might be related to the longer seed used or simply to some machine instabilities, an exhaustive explanation has not been found yet and we are going to experimentally investigate it in details in the next future.

Bibliography

[1] P. G. O'Shea and H. P. Freund, Free-Electron Lasers: Status and applications, Science 8, Vol. 292 no. 5523 pp. 1853-1858

[2] LEUTL, http://www.aps.anl.gov./aod/mcrops

[3] VISA, http://lcls.slac.stanford.edu/

[4] Tesla Test Facility, http://tesla-new.desy.de

[5] T. Shintake, Status of the SCSS Prototype Accelerator and XFEL Project in Japan, Talk at the EPAC conference 2006 , Switzerland

[6] LCLS, http://lcls.slac.stanford.edu/

[7] FERMI, http://www.elettra.trieste.it/FERMI/

[8] J. Urbančič, Studies for the commissioning of FERMI@Elettra: A Free electron laser based on the principle of seeded harmonic generation, Master Thesis, 2011

[9] M. Hosaka et. al., High POWER DEEP UV LASING ON THE UVSOR-II STORAGE RING FEL, Proceedings of FEL 2006, BESSY, Berlin, Germany

[10] Elettra SRFEL, http://www.elettra.trieste.it/it/lightsources/elettra/elettra-beamlines/fel/fel.html

[11] S. Y. Lee, Accelerator physics, second edition, World Scientific Publishing Company, 2007

[12] P. M. Lapostolle, A. L. Septier (Eds.), Linear accelerators, North-Holland Publ. Co, Amsterdam (1970)

[13] M. Vretenar, Introduction to linear accelerators, CERN Accelerator School, Varna 2010.

[14] M. Benoît, Coherence, tunability, spectral and spatial properties of femtosecond extreme-ultraviolet light sources, Ph.D. Dissertation, Paris (2013)

[15] H. Wiedemann, Particle Accelerator Physics, Third Edition, Springer, 2007

[16] E. Allaria et al., Highly coherent and stable pulses from the FERMI seeded free-electron laser in the extreme ultraviolet, Nature Photonics Vol 6, 699-704 (2012); DOI:10.1038/nphoton.2012.233

[17] C. J. Bocchetta, et al., "FERMI@Elettra CDR", http://www.elettra.trieste.it/FERMI, (2007)

[18] G. Penco et al., Optimization of a high brightness photoinjector for a seeded FEL facility, JINST 8, P050015 (2013)

[19] S. Di Mitri et al., Design and simulation challenges for FERMI@elettra, Nucl. Instrum. Methods Phys. Res., Sect. A, 608, 19 (2009)

[20] M. Zangrando et al., The photon analysis, delivery, and reduction system at the FERMI@Elettra free electron laser user facility, Rev. Sci. Instrum. 80, 113110 (2009)

[21] P. Emma, X-Band RF Harmonic Compensation for Linear Bunch Compression in the LCLS, LCLS-TN-01-1 , SLAC November 14, 2001

[22] F. Capotondi et al., Coherent imaging using seeded free-electron laser pulses with variable polarization: First results and research opportunities, Rev. Sci. Instrum. 84, 051301 (2013)

[23] B. E. A. Saleh and M. C. Teich, Fundamentals of Photonics (Wiley, 2007)

[24] G. De Ninno et al., Chirped seeded free-electron lasers: self standing light sources for two color pump probe experiments, Phys. Rev. Lett. 110, 064801 (2013)

[25] E. Allaria et al., Spectral characterization of the FERMI pulses in the presence of electron-beam phase-space modulations, Proceedings of FEL 2012, Nara, Japan

[26] G.Penco et al., Time-sliced emittance and energy spread measurements at FERMI@Elettra, Proceedings of FEL 2012, Nara, Japan

[27] P. Craievch et al., RF Deflection of the Electron Bunch at High Energy in FERMI@Elettra, ST/F-TN-07/09

[28] A. A. Lutman et al., Impact of an initial energy chirp and an initial energy curvature on a seeded free electron laser: free electron laser properties (2009), Journal of Physics A: Mathematical end Theoretical 42, 085405

[29] G. Stupakov, Compensation of laser frequency chirp in seeding with beam energy profile, Presentation at SSSFEL12 workshop, Trieste, Italy December 10-12, 2012

[30] J. Wu et al., Interplay of the chirps and chirped pulse compression in a high-gain seeded free-electron laser, JOSA B, Vol. 24, Issue 3, pp. 484-495 (2007)

[31] A.A. Lutman et al., Impact of an initial energy chirp and an initial energy curvature on a seeded free electron laser: the Green Function, (2008) J. Phys. A: Math. Theor. 42, 045202

[32] D.Gauthier, private communication, september 2013